

Are We Overlooking the Dimensions? Learning Latent Hierarchical Channel Structure for High-Dimensional Time Series Forecasting

Juntong Ni*, Shiyu Wang*†, Zewen Liu, Xiaoming Shi, Xinyue Zhong, Zhou Ye, Wei Jin
Emory University
{juntong.ni, zewen.liu, wei.jin}@emory.edu, kwuking@gmail.com

Abstract

Time series forecasting (TSF) is a central problem in time series analysis. However, as the number of channels in time series datasets scales to the thousands or more, a scenario we define as **High-Dimensional Time Series Forecasting (HDTSF)**, it introduces significant new modeling challenges that are often not the primary focus of traditional TSF research. HDTSF is challenging because the channel correlation often forms complex and hierarchical patterns. Existing TSF models either ignore these interactions or fail to scale as dimensionality grows. To address this issue, we propose U-CAST, a channel-dependent forecasting architecture that learns latent hierarchical channel structures with an innovative query-based attention. To disentangle highly correlated channel representation, U-CAST adds a full-rank regularization during training. We also release TIME-HD, a benchmark of large, diverse, high-dimensional datasets. Our theory shows that exploiting cross-channel information lowers forecasting risk, and experiments on TIME-HD demonstrate that U-CAST surpasses strong baselines in both accuracy and efficiency. Together, U-CAST and TIME-HD provide a solid basis for future HDTSF research. To promote reproducibility and future extensions, we release TIME-HD-LIB at GitHub, and TIME-HD can be accessed at Hugging Face.

1 Introduction

Time series data involving multiple variables (a.k.a. channels) that change over time are fundamental to numerous real-world applications, such as stock market prices [17], highway traffic flows [52], solar power generation outputs [43], and temperature measurements [50]. Consequently, time series forecasting (TSF) has become a central challenge in the time series analysis community, aiming to predict future values based on historical observations [5, 12]. Recent advances in machine learning have catalyzed significant methodological progress in this field [45, 22], leading to a variety of novel architectures [49, 59, 58, 25, 36, 35, 44, 48, 34, 13, 57]. These models can be broadly categorized by how they handle the inter-channel dependencies: channel-dependent (CD) methods [25, 54, 49, 58, 6, 59] explicitly capture cross-variable interactions, while channel-independent (CI) methods [35, 53, 10, 44, 51, 23] treat each variable separately.

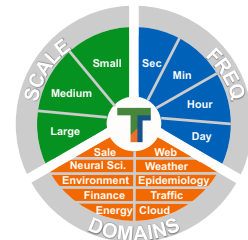


Figure 1: TIME-HD provides diverse high-dimensional datasets.

*Equal contribution

†Project lead

However, as the number of channels in time series datasets scales into the thousands or more, a scenario we define as **High-Dimensional Time Series Forecasting (HDTSF)** has posed significant new modeling challenges that are often not the primary focus of traditional TSF research. In the HDTSF regime, the sheer volume of channels can complicate the channel dependency patterns and render traditional models, which are often developed and evaluated on low-dimensional datasets, computationally infeasible or unreliable. More importantly, high dimensionality often gives rise to latent hierarchical structures within the channels. These structures are common in large real-world systems, where channels exhibit implicit groupings and multi-level correlations based on factors such as spatial proximity (e.g., nested geographical regions in climate data) or semantic relationships (e.g., stocks within related economic sub-sectors). While some explicit hierarchies might be known, many are latent and can evolve dynamically. Existing TSF models are often not designed to discover or leverage these complex, multi-scale hierarchical channel dependencies, which may significantly limit their generalizability in high-dimensional contexts.

To address the specific challenge of effectively modeling these latent hierarchical channel structures within HDTSF, we propose **U-CAST**, a novel and efficient forecasting model that incorporates an innovative query-based attention mechanism within a Hierarchical Latent Query Network and a Hierarchical Upsampling Network. This architecture is expressly designed to infer latent hierarchical organizations among channels and efficiently compute multi-scale correlations. To further enhance the distinctiveness of learned representations within this hierarchy, especially when dealing with highly correlated raw channel data, U-CAST employs a full-rank regularization technique.

Developing and rigorously evaluating methods like U-CAST, which are tailored for the intricacies of HDTSF and its characteristic hierarchical dependencies, requires datasets that adequately reflect these complexities. However, commonly used TSF benchmarks (e.g., ETT [58], WEATHER [49]) often feature a limited number of channels and may not possess the scale or structural richness representative of many emerging high-dimensional applications. This gap can hinder the robust assessment of model scalability, the nuanced benefits of sophisticated dependency modeling strategies, and overall generalizability. To facilitate rigorous research in HDTSF and provide a suitable testbed for U-CAST and future innovative approaches, we have curated **TIME-HD**. TIME-HD is the first comprehensive benchmark suite specifically focused on high-dimensional time series, offering large-scale, domain-diverse datasets, as illustrated in Figure 1. Our experiments on TIME-HD validate U-CAST’s efficacy in learning hierarchical structures and achieving superior forecasting accuracy in these demanding high-dimensional settings. Our main contributions are summarized as:

C1: Detailed analysis of channel dependency. We provide rigorous theoretical and empirical evidence (Section 3) that highlights the importance of effectively modeling inter-channel dependencies for time series forecasting. It shows that CD can achieve lower Bayes risk than CI, and that incorporating more relevant channels can further improve forecasting accuracy, highlighting the need for high-dimensional benchmark datasets.

C2: A strong model for high-dimensional time series forecasting. We propose U-CAST (Section 4), a new CD forecasting model that employs an innovative query-based attention mechanism to efficiently learn latent hierarchical channel structures and enables scalable modeling of inter-channel correlations. U-CAST combines strong performance across TIME-HD with the best efficiency among baselines, making it a reference point for future models.

C3: A large-scale high-dimensional time series forecasting benchmark. We release TIME-HD (Section 5), the first comprehensive benchmark suite specifically focused on high-dimensional time series forecasting. These datasets, characterized by substantial scale and broad domain representation, are systematically collected, curated, and preprocessed to offer a realistic and challenging testbed for evaluating model scalability and generalizability. We observe that CD methods do not consistently outperform CI methods, likely because current CD baselines either fail to capture complex channel dependencies or do not scale to high-dimensional time series.

C4: An open-source toolkit for reproducible research. To cultivate a collaborative research ecosystem, we release TIME-HD-LIB. This open-source library provides an end-to-end framework supporting the TIME-HD benchmark, including standardized data preprocessing, seamless integration of datasets, unified evaluation protocols, and facilities for hyperparameter optimization, thus promoting reproducibility and future extensions.

2 Related Work

High-Dimensional Time Series Datasets. Some high-dimensional datasets have already been used in recent work on building time series foundation models [47, 1, 40, 16]. These studies primarily focus on leveraging high-dimensional datasets for pretraining. However, several limitations exist in how they handle such datasets. **First**, during pretraining, channels are treated independently, capturing only temporal dependencies without modeling inter-channel correlations. **Second**, despite pretraining on high-dimensional datasets, fine-tuning and evaluation are still performed on low-dimensional ones. **Third**, some pretraining datasets have unaligned timestamps, complicating their use in evaluation. These limitations highlight the importance of developing high-dimensional time series datasets specifically tailored for benchmarking and evaluation in time series forecasting research. Table 5 in Appendix A provides a more detailed summarization of the differences between TIME-HD and existing works.

Multivariate Time Series Forecasting. Previous methods for modeling multivariate time series can be broadly categorized into **channel-independent (CI)** and **channel-dependent (CD)** strategies. The CI modeling strategy employs a shared model backbone across all channels and processes each channel independently during the forward pass [35, 53, 51, 44, 42, 10, 23]. This design typically results in lower model capacity but offers greater robustness. In contrast, the CD modeling strategy introduces dedicated modules to capture inter-channel dependencies. Based on the granularity at which these correlations are modeled, CD can be further divided into position-wise [7, 48, 49, 58, 59, 54], token-wise [25, 46], and cluster-wise [6, 39] approaches. These methods are expected to provide higher capacity and make better use of cross-channel information. However, due to the constraints of existing low-dimensional multivariate time series forecasting benchmarks, most methods have not been validated at scale. We provide a more detailed discussion in Appendix A.

3 Preliminary Study

Prior studies on existing time series benchmarks, which are often of low dimensionality, do not consistently show a clear advantage of CD over CI models [55, 35, 53, 10, 56]. This observation might lead to skepticism regarding the practical benefits of explicitly modeling inter-channel correlations. However, we hypothesize that the limited dimensionality of these benchmarks inherently restricts the potential gains from CD approaches. This preliminary study aims to theoretically and empirically investigate the impact of data dimensionality on the forecasting performance achievable by leveraging channel correlations. We begin with a theoretical analysis of risk reduction.

Task Formulation. For time series forecasting, given an input time series $\mathbf{X} \in \mathbb{R}^{C \times T}$, where T represents the length of the look-back window and C represents the number of variables, the goal is to predict the future S time steps $\mathbf{Y} \in \mathbb{R}^{C \times S}$.

3.1 Theoretical Analysis of Risk Reduction from CD Models

To formally analyze the benefits of CD modeling, we consider a simplified setting. Assume a **bivariate** time series ($C = 2$) generated by a Vector Autoregression process of order 1 (VAR(1)) [41]:

$$z_{t+1} = \mathbf{A}z_t + \varepsilon_{t+1}, \quad \mathbf{A} = \begin{pmatrix} a_{11} & a_{12} \\ a_{21} & a_{22} \end{pmatrix}, \quad \varepsilon_t \stackrel{i.i.d.}{\sim} \mathcal{N}(\mathbf{0}, \Sigma), \quad \Sigma = \begin{pmatrix} \sigma_{11} & 0 \\ 0 & \sigma_{22} \end{pmatrix}. \quad (1)$$

Here, $z_t = (z_t^{(1)}, z_t^{(2)})^\top$ is the bivariate time series value at time t , with $z_0 \sim \mathcal{N}(\mathbf{0}, \mathbf{I})$, where \mathbf{I} is the identity matrix. The matrix \mathbf{A} captures the linear dependencies, with coefficients a_{ij} describing self-dependencies ($i = j$) and cross-dependencies ($i \neq j$). The noise ε_t is zero-mean Gaussian with independent components. Our goal is to predict z_{t+1} given z_t . All time series are assumed to be normalized to have zero mean. We compare two modeling strategies under squared-error loss: (1) *CI Modeling*: Each channel $z_{t+1}^{(i)}$ is predicted using only its own past, $z_t^{(i)}$. The Bayes optimal forecast for $z_{t+1}^{(i)}$ is $\mathbb{E}[z_{t+1}^{(i)} | z_t^{(i)}]$ and the total risk is $R_{CI} = \sum_{i=1}^2 \mathbb{E}[(z_{t+1}^{(i)} - \mathbb{E}(z_{t+1}^{(i)} | z_t^{(i)}))^2]$. (2) *CD Modeling*: Each channel $z_{t+1}^{(i)}$ is predicted using the past of all channels. The Bayes optimal forecast for $z_{t+1}^{(i)}$ is $\mathbb{E}[z_{t+1}^{(i)} | z_t]$ and the total risk is $R_{CD} = \sum_{i=1}^2 \mathbb{E}[(z_{t+1}^{(i)} - \mathbb{E}(z_{t+1}^{(i)} | z_t))^2]$.

Theorem 1 (Risk Reduction from CD). *For the time series described in Eq. (1), the Bayes risks of CI and CD models under squared-error loss satisfy: $R_{CI} - R_{CD} \geq 0$. This inequality is strict if and only*

if $a_{12} \neq 0$ and $a_{21} \neq 0$, and the conditional variances $\text{Var}(z_t^{(1)} | z_t^{(2)})$ (representing the variance of $z_t^{(1)}$ that remains after $z_t^{(2)}$ is known) and $\text{Var}(z_t^{(2)} | z_t^{(1)})$ are positive.

We provide the proof of this theorem in Appendix E. Theorem 1 establishes that CD modeling is at least as good as CI modeling. A strict advantage for CD arises if: (1) there is genuine predictive information flowing between channels (non-zero a_{12} or a_{21} means one channel directly influences the future of the other), and (2) each channel contains some unique information not present in the other (positive conditional variances). If channels are truly independent in their evolution ($a_{12} = a_{21} = 0$) or one is a deterministic function of the other, then $R_{\text{CI}} = R_{\text{CD}}$.

To investigate the impact of increasing dimensionality, we now consider a general P -channel VAR(1) process: $z_{t+1} = \mathbf{A}z_t + \varepsilon_{t+1}$, where $z_t \in \mathbb{R}^P$. We focus on forecasting a single target channel, say $Y = z_{t+1}^{(1)}$, which is given by $z_{t+1}^{(1)} = \sum_{j=1}^P a_{1j}z_t^{(j)} + \varepsilon_{t+1}^{(1)}$, with $\text{Var}(\varepsilon_{t+1}^{(1)}) = \sigma_{11}$. Let R_p denote the Bayes risk (minimum MSE) for forecasting $Y = z_{t+1}^{(1)}$ using the information from the first p channels at time t , i.e., $\{z_t^{(1)}, \dots, z_t^{(p)}\}$.

Theorem 2 (Bayes Risk Monotonicity with Increasing Channel Information). *For forecasting the target channel $z_{t+1}^{(1)}$, the Bayes risks obtained by conditioning on an increasing number of predictor channels $\{z_t^{(1)}, \dots, z_t^{(p)}\}$ exhibit monotonicity: $R_1 \geq R_2 \geq \dots \geq R_P = \sigma_{11}$. Note that R_1 is the risk of CI Modeling (using only $z_t^{(1)}$ to predict $z_{t+1}^{(1)}$), and R_p ($p > 1$) is the risk of CD Modeling. Furthermore, the risk difference between CI and CD, $\Delta_p = R_1 - R_p$, is non-decreasing in p :*

$$0 = \Delta_1 \leq \Delta_2 \leq \dots \leq \Delta_P = R_1 - \sigma_{11},$$

This gap strictly increases (i.e., $\Delta_p > \Delta_{p-1}$) if and only if the p -th channel, $z_t^{(p)}$, provides new information for predicting Y that is not already contained in channels $z_t^{(1)}, \dots, z_t^{(p-1)}$.

The proof is provided in Appendix F. Theorem 2 formally shows that incorporating additional informative and non-redundant channels progressively reduces the forecasting risk for a target variable. This underscores the theoretical benefit of using more relevant dimensions (channels), supporting our hypothesis that higher-dimensional data provides greater opportunity for CD models to outperform CI approaches.

3.2 Empirical Analysis

Table 1: MSE for CI and CD models under different settings.

Model	Independent 100	Anti-Self 100	Anti-Self 250	Anti-Self 2000
CI	0.0043	0.0052	0.0054	0.0054
CD	0.0066	0.0014	0.0012	0.0011

To empirically validate our theoretical insights above, we conduct controlled experiments on synthetic data for evaluating the performance difference between CI and CD modeling under varying channel-dependency structures and dimensionalities.

Data Generation. We generate synthetic multivariate time series using a C -dimensional Vector Autoregression process in Equation 1, where the coefficient matrix $\mathbf{A} \in \mathbb{R}^{C \times C}$ encodes the dependency structure of channels. We focus on two distinct structures for \mathbf{A} : (1) **Independent**: Channels evolve independently of each other i.e., \mathbf{A} is a diagonal matrix. For this setting, we use $C = 100$ channels. (2) **Anti-Self**: Channels depend significantly on other channels but not on their own immediate past, i.e., \mathbf{A} has zero diagonal entries and non-zero off-diagonal entries. To examine the impact of dimensionality, we generate Anti-Self datasets with $C \in \{100, 250, 2000\}$. More experimental details are provided in Appendix I.

Forecasting Models. To isolate the core impact of utilizing versus disregarding channel dependencies, we employ two simple linear forecasting architectures: (1) **CI**: A single univariate linear model is fitted for each channel using only its own past values. (2) **CD**: A linear model is applied along the channel dimension to incorporate inter-channel dependencies.

Results and Discussion. As shown in Table 1, the CI model performs better in the Independent setting, where no inter-channel dependencies exist. In contrast, in all Anti-Self settings, the CD

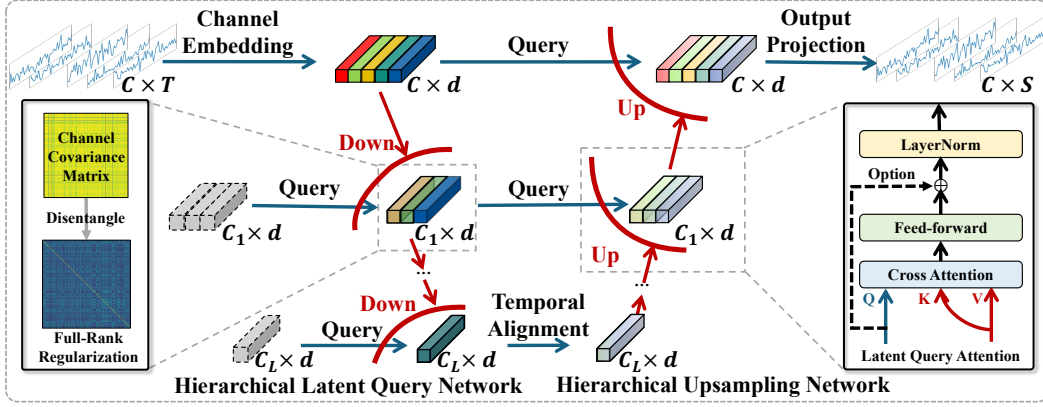


Figure 2: Overall framework of U-CAST, which consists of five main modules: channel embedding, hierarchical latent query, temporal alignment, hierarchical upsampling, and output projection.

model achieves substantially lower MSE with larger gains as the number of interacting channels increases. These empirical findings are consistent with our theoretical analysis: CD modeling becomes increasingly effective when significant inter-channel dependencies exist, especially in higher-dimensional systems. These observations highlight a pressing need for progress on two critical fronts. First, there is a clear demand for **novel CD models** capable of efficiently and effectively navigating the intricacies of high-dimensional time series data. Second, the development of dedicated **high-dimensional forecasting benchmarks**, characterized by complex channel dependencies, is crucial for the rigorous evaluation and continued advancement of such sophisticated methods. Accordingly, in the subsequent sections, we address these needs by first introducing our U-CAST framework specifically tailored for HDTSF and then presenting TIME-HD, a comprehensive benchmark designed to support and galvanize further research in this evolving domain.

4 U-CAST Framework

Our theoretical and empirical analyses in Section 3 highlight the need for novel CD models that can efficiently handle high-dimensional time series. Traditional models often struggle with scalability and overlook the structured nature of such data, especially *hierarchical* correlations among variable groups. To address this, we propose U-CAST (see Figure 2), an efficient model that captures channel correlations via learning latent hierarchical structures. We also introduce a full-rank regularization term to encourage disentanglement and improve the learning of structured representations.

4.1 Model Architecture

Channel Embedding. The input sequence is first normalized. A linear projection $\mathbf{W}_{\text{in}} \in \mathbb{R}^{T \times d}$ converts the temporal dimension to a hidden dimension d :

$$\mathbf{H}^{(0)} = \mathbf{X}\mathbf{W}_{\text{in}} \in \mathbb{R}^{C \times d}. \quad (2)$$

Hierarchical Latent Query Network. Self-attention is well suited to modelling channel-wise dependencies because every variable can attend to every other variable without assuming locality. However, applying full attention to C channels incurs quadratic cost, which is prohibitive when C is large. Hierarchical latent query network addresses this by introducing a set of *latent queries* that serve as an information bottleneck. At layer $\ell \in \{1, \dots, L\}$ the number of latent queries is $C_\ell = \lfloor C/r^\ell \rfloor$, where $r > 1$ is a pre-defined *reduction ratio*. The queries are shared across samples: $\mathbf{Q}_\ell \in \mathbb{R}^{C_\ell \times d}$. The Latent Query Attention at layer ℓ is

$$\begin{aligned} \mathbf{Q} &= W_q \mathbf{Q}_\ell, \quad \mathbf{K} = W_k \mathbf{H}^{(\ell-1)}, \quad \mathbf{V} = W_v \mathbf{H}^{(\ell-1)}, \\ \mathbf{H}^{(\ell)} &= W_o \left(\text{softmax} \left(\frac{\mathbf{Q}\mathbf{K}^\top}{\sqrt{d_h}} \right) \mathbf{V} \right) \in \mathbb{R}^{C_\ell \times d}, \end{aligned} \quad (3)$$

followed by layer normalisation. Successive layers hierarchical latent query network builds a hierarchy in which higher-level queries summarise wider channel groups.

Temporal Alignment. The deepest latent representation $\mathbf{H}^{(L)} \in \mathbb{R}^{C_L \times d}$ stores C_L latent channel tokens whose d -dimensional feature vectors encode the *temporal* dynamics extracted from the look-back window. To keep these temporal features coherent when the model switches from down-sampling to up-sampling, we apply a shared linear predictor f_{pred} along the temporal dimension:

$$\mathbf{U}^{(L)} = f_{\text{pred}}(\mathbf{H}^{(L)}) \in \mathbb{R}^{C_L \times d}. \quad (4)$$

Hierarchical Upsampling Network. Forecasting demands channel-wise outputs of size C , so the hierarchy is traversed in reverse to restore resolution. At layer $\ell = L, \dots, 1$ the Up-Latent Query Attention uses the representation from the encoder as queries and the current decoder representation as keys and values:

$$\begin{aligned} \mathbf{Q} &= \mathbf{W}_q \mathbf{H}^{(\ell-1)}, \quad \mathbf{K} = \mathbf{W}_k \mathbf{U}^{(\ell)}, \quad \mathbf{V} = \mathbf{W}_v \mathbf{U}^{(\ell)}, \\ \mathbf{U}^{(\ell-1)} &= \mathbf{W}_o \left(\text{softmax} \left(\frac{\mathbf{Q}\mathbf{K}^\top}{\sqrt{d_h}} \right) \mathbf{V} \right) + \mathbf{H}^{(\ell-1)} \in \mathbb{R}^{C_{\ell-1} \times d}. \end{aligned} \quad (5)$$

The skip connection $\mathbf{H}^{(\ell-1)}$ guides the reconstruction, ensuring that the original channel information is recovered with minimal distortion.

Output Projection. After upsampling $\mathbf{U}^{(0)} \in \mathbb{R}^{C \times d}$ has the same channel dimension as the encoder output $\mathbf{H}^{(0)}$. A residual link followed by a projection yields the horizon-length prediction:

$$\hat{\mathbf{Y}} = (\mathbf{U}^{(0)} + \mathbf{H}^{(0)}) \mathbf{W}_{\text{out}}, \quad \mathbf{W}_{\text{out}} \in \mathbb{R}^{d \times S}. \quad (6)$$

Finally, we apply the inverse of the initial normalisation to obtain the forecast in the original scale.

4.2 Optimization Objective

Full-Rank Regularization. Representation learning is fundamentally about *disentanglement*: channels are highly correlated in the high-dimensional time series data (see Table 2). This entanglement means that the latent matrix $\mathbf{H}^{(\ell-1)} \in \mathbb{R}^{C \times d}$ often has rank $r = \text{rank}(\mathbf{H}^{(\ell-1)}) \ll C$. The resulting rank deficiency signals redundancy among channels and obscures the latent hierarchical channel structure. Achieving disentanglement is therefore required to learn this structure. To resolve this issue, we introduce a full-rank regularization, whose effect is formalised in Theorem 3 below.

Theorem 3 (Full-Rank Regularisation). *Let $\mathbf{H}^{(\ell-1)} \in \mathbb{R}^{C \times d}$ be of rank $r < \min(C, d)$. Let $\mathbf{Q} \in \mathbb{R}^{C' \times C}$ be learnable, full row rank, and $C' \leq r$. Define $\mathbf{H}^{(\ell)} = \mathbf{Q}\mathbf{H}^{(\ell-1)} \in \mathbb{R}^{C' \times d}$. There exists a choice of \mathbf{Q} such that $\text{rank}(\mathbf{H}^{(\ell)}) = C'$. Further, if $r \geq d$ and $C' \geq d$, adding a full-rank regulariser (e.g. the log-determinant of $\mathbf{H}^{(\ell)}\mathbf{H}^{(\ell)\top}$) drives $\mathbf{H}^{(\ell)}$ toward row rank $\min(C', d)$.*

The proof is given in Appendix G. Theorem 3 states that enforcing full rank on $\mathbf{H}^{(\ell)}$ is sufficient to remove linear redundancy among channels and reveal a clear hierarchical latent channel structure. Define the row-covariance matrix $\boldsymbol{\Sigma}^{(\ell)} = \frac{1}{d} \mathbf{H}^{(\ell)}\mathbf{H}^{(\ell)\top} \in \mathbb{R}^{C' \times C'}$. The log-determinant $\log \det(\boldsymbol{\Sigma}^{(\ell)} + \varepsilon I_{C'})$ is proportional to the generalised variance³. Maximising this value keeps every eigenvalue bounded away from zero, so the channel vectors occupy a larger subspace and share less redundant information. We thus define the full-rank regularization loss as

$$\mathcal{L}_{\text{cov}}^{(\ell)} = -\frac{1}{C'} \log \det(\boldsymbol{\Sigma}^{(\ell)} + \varepsilon I_{C'}),$$

where $\varepsilon I_{C'}$ ensures positive definiteness and stabilizes early training. The $1/C'$ factor removes scale dependence, simplifying the weighting of this term. The overall loss is the average over all L layers. Minimizing \mathcal{L}_{cov} increases the Shannon differential entropy (Theorem 4), reducing redundancy and promoting disentanglement by encouraging each channel to carry distinct information.

Overall Objective. The model parameters are learned by minimising the combined loss

$$\mathcal{L} = \mathcal{L}_{\text{mse}} + \alpha \mathcal{L}_{\text{cov}}, \quad (7)$$

where \mathcal{L}_{mse} is the supervised mean-squared forecasting error, \mathcal{L}_{cov} is the layer-averaged covariance penalty, and α controls the strength of this regulariser.

Table 2: TIME-HD descriptions. The calculation of Correlation is illustrated in Appendix L.

Dataset	Dimensions	Dataset Size	Frequency	Pred Length	Storage	Domains	Correlation
Neurolib	2,000	60,000	1 ms	336	2.44 GB	Neural Science	0.926±0.007
Solar	5,162	105,120	5 Mins	336	2.33 GB	Energy	0.998±0.000
Atec	1,569	8,928	10 Mins	336	158.8 MB	Cloud	0.851±0.036
Meter	2,898	28,512	30 Mins	336	651 MB	Energy	0.864±0.023
Temp	3,850	17,544	1 Hour	168	383.6 MB	Weather	0.833±0.039
Wind	3,850	17,544	1 Hour	168	331.4 MB	Weather	0.937±0.011
Traffic-CA	7,491	43,824	1 Hour	168	2.48 GB	Traffic	0.962±0.009
Traffic-GLA	3,376	43,824	1 Hour	168	1.12 GB	Traffic	0.947±0.012
Traffic-GBA	2,229	43,824	1 Hour	168	689.1 MB	Traffic	0.978±0.003
Air Quality	1,105	15,461	6 Hours	28	94.6 MB	Environment	0.854±0.030
SIRS	2,994	9,000	1 Day	7	675 MB	Epidemiology	0.991±0.002
SP500	1,475	7,553	1 Day	7	184.1 MB	Finance	0.738±0.046
M5	3,049	1,941	1 Day	7	13.7 MB	Sale	0.726±0.073
Measles	1,161	1,330	1 Day	7	12.1 MB	Epidemiology	0.724±0.048
Wiki-20k	20,000	2,557	1 Day	7	289 MB	Web	0.923±0.017
Mobility	5,826	974	1 Day	7	29.7 MB	Social	0.847±0.027

5 TIME-HD: High-Dimensional Time Series Forecasting Benchmark

The goal of TIME-HD is to support and advance research in time series forecasting, which is a rapidly growing and increasingly important area. Details on datasets generation, collection, and cleaning are provided in Appendix K. As shown in Table 2 and Figure 1, TIME-HD has several key characteristics:

- **High Dimensionality.** TIME-HD includes 16 high-dimensional time series forecasting datasets. The number of variables (dimensions) in these datasets ranges from 1,161 to 20,000, which is significantly larger than in commonly used benchmarks such as ETT, Weather, ECL, Solar, and Traffic (which typically have 7–862 channels). These high-dimensional datasets provide opportunities for developing scalable methods, enable exploration of channel-dependent models, and allow for more robust performance evaluations.
- **Diverse Sources.** TIME-HD comprises both simulated and real-world datasets. *Neurolib* and *SIRS* are simulated using domain-informed differential equations and are valuable for scientific modeling and hypothesis testing. The remaining datasets are based on real-world observations, making them suitable for evaluating the generalization ability of forecasting models in practical settings. The inclusion of both types enables comprehensive performance assessments.
- **Varied Scales.** TIME-HD offers datasets of different sizes, defined by the number of variables and temporal length. Disk memory usage reflects this variability. As indicated in Table 2, there are 4 large-scale (gigabyte-level), 8 medium-scale (hundreds of megabytes), and 4 small-scale (tens of megabytes) datasets. The small and medium-scale datasets fit in the memory of a single GPU, making them suitable for evaluating resource-intensive models. The large-scale datasets support research on scalable methods using mini-batching and distributed training.
- **Different Sampling Frequencies.** TIME-HD covers a range of sampling frequencies, including milliseconds, minutes, hours, and days (see Table 2). This variety reflects real-world conditions across application domains and enables evaluation across different temporal resolutions. Furthermore, TIME-HD uses frequency-specific prediction lengths that are more realistic than fixed-length horizons commonly used in previous benchmarks.
- **Broad Domain Coverage.** TIME-HD includes datasets from 10 diverse domains, such as neural science, energy, cloud computing, weather, traffic, epidemiology, finance, and social behavior. This diversity supports the development of general-purpose forecasting models and enables comparison against domain-specific approaches.

Channel Correlation Statistic. We follow TFB [38] to compute channel correlation. The results are shown in the “Correlation” column of Table 2. All datasets exhibit high average channel correlation, confirming the presence of strong inter-variable dependencies in these high-dimensional time series. The details of correlation calculation is illustrated in Appendix L.

³Product of the eigenvalues of $\Sigma^{(\ell)}$.

Table 3: Forecasting results on various datasets. The prediction length of each dataset is described in Table 2. A lower MSE or MAE indicates better performance. The best performance is highlighted in **red**, and the second-best is **underlined**.

Models	Channel-Independent						Channel-Dependent											
	DLinear		PAttn		PatchTST		iTransformer		TSMixer		TimesNet		CCM		DUET		U-CAST	
	MSE	MAE	MSE	MAE	MSE	MAE	MSE	MAE	MSE	MAE	MSE	MAE	MSE	MAE	MSE	MAE	MSE	MAE
Atec	0.318	0.314	0.299	0.275	<u>0.298</u>	0.298	0.345	0.319	0.398	0.387	0.493	0.429	0.362	0.346	0.330	0.339	0.287	0.280
Air Quality	0.449	0.446	0.449	0.432	0.448	0.432	<u>0.447</u>	<u>0.431</u>	0.447	0.438	0.457	0.438	0.458	0.451	0.452	0.444	0.446	0.430
Temp	0.272	0.391	0.278	0.395	0.279	0.396	<u>0.265</u>	0.386	0.266	0.389	0.287	0.408	0.279	0.398	0.435	0.511	0.262	0.383
Wind	1.128	<u>0.697</u>	1.256	0.758	1.254	0.757	<u>1.116</u>	0.699	1.346	0.742	1.161	0.708	1.165	0.698	1.227	0.746	1.104	0.692
Mobility	0.344	0.359	0.337	0.336	0.344	0.341	0.312	0.314	1.165	0.787	0.410	0.388	0.523	0.468	0.439	0.410	<u>0.315</u>	<u>0.317</u>
Traffic-CA	<u>0.063</u>	<u>0.141</u>	0.491	0.554	0.295	0.417	0.271	0.391	0.082	0.186	0.101	0.205	0.067	0.153	—	—	0.061	0.131
Traffic-GBA	0.062	0.137	<u>0.059</u>	<u>0.132</u>	0.060	0.139	0.063	0.141	0.074	0.168	0.098	0.204	0.067	0.151	0.650	0.638	0.059	0.126
Traffic-GLA	0.062	0.142	<u>0.060</u>	0.136	0.060	<u>0.136</u>	0.065	0.145	0.071	0.168	0.094	0.199	0.066	0.152	0.810	0.738	0.060	0.132
M5	3.688	0.870	3.650	0.867	3.655	0.872	<u>3.549</u>	<u>0.853</u>	6.863	1.623	4.490	0.919	4.916	0.941	3.768	0.880	3.501	0.849
Measles	0.128	0.252	0.011	0.048	0.013	0.058	<u>0.010</u>	<u>0.048</u>	0.569	0.547	0.018	0.060	0.244	0.323	0.015	0.064	0.010	0.042
Neurolib	1.793	0.381	2.458	0.445	2.395	0.438	1.718	0.347	2.240	0.532	2.475	0.458	1.774	0.403	2.519	0.451	<u>1.750</u>	<u>0.350</u>
Solar	0.174	0.255	0.604	0.582	0.416	0.469	0.343	0.427	0.155	0.216	<u>0.157</u>	<u>0.224</u>	0.177	0.258	—	—	0.172	0.246
SIRS	0.058	0.168	<u>0.025</u>	<u>0.109</u>	0.033	0.129	0.028	0.113	0.016	0.078	0.162	0.327	0.048	0.156	0.095	0.236	0.007	0.052
Meters	0.944	0.549	0.941	0.552	1.254	0.706	0.949	0.506	0.987	0.564	1.034	0.586	0.946	0.551	1.308	0.731	<u>0.943</u>	<u>0.551</u>
SP500	0.630	0.367	<u>0.516</u>	<u>0.309</u>	0.523	0.313	0.511	0.306	2.674	1.120	0.611	0.343	0.727	0.414	0.568	0.335	0.555	0.328
Wiki-20k	10.740	0.394	10.290	0.306	<u>10.291</u>	<u>0.305</u>	10.933	0.405	10.446	0.332	10.586	0.325	11.413	0.373	10.278	0.304	10.273	0.302
1st Count	0	1	1	1	0	0	<u>3</u>	<u>3</u>	1	1	0	0	0	0	0	0	11	10

6 Experiment Results and Framework Analysis

Baselines. We consider the following representative models as our baselines for HDTSF:

- Channel-Independent.** We include three methods that employ a shared model backbone across all channels: **DLinear** [53], **PAttn** [42], and **PatchTST** [35]. These methods use linear projection, attention mechanisms, and the Transformer architecture, respectively, to model temporal dependencies.
- Channel-Dependent.** We adopt five methods that incorporate dedicated modules to capture inter-channel dependencies. **TimesNet** [48] and **TSMixer** [7] are position-wise methods that capture channel correlations at each time step by embedding. **iTransformer** [25] is a token-wise method that treats the entire time series of each channel as a token and models inter-channel dependencies using a Transformer. Additionally, we consider two clustering-based methods: **CCM** [6] and **DUET** [39], which explicitly group highly correlated channels into clusters and model dependencies within each cluster.

Benchmark Results. The experimental setup is detailed in Appendix M. The results are shown in Table 3. We summarize the following observations from our benchmark results: **First**, although CI methods cannot explicitly model channel correlations, they are designed to learn shared temporal patterns across channels. This can help reduce the risk of overfitting, enabling CI methods to achieve competitive performance. Among them, PAttn generally achieves better results, indicating the effectiveness of attention mechanisms for temporal modeling. **Second**, among CD methods, iTransformer significantly outperforms others, suggesting that treating each channel as a token and using attention to model inter-channel dependencies is more effective than position-wise or cluster-based approaches in high-dimensional settings. We argue that the token-wise design helps mitigate noise in the temporal dimension and fully utilizes the benefits of the attention mechanism. **Third**, CD methods do not show a consistent or significant performance advantage over CI methods. However, our theoretical analysis in Section 3 suggests that CD can reduce the MSE risk compared to CI in multivariate time series forecasting. We believe this is due to current CD baselines either failing to effectively exploit complex channel dependencies or being unable not scale to high-dimensional time series.

Performance Gains of U-CAST. As shown in Table 3, U-CAST achieves top performance on the high-dimensional TIME-HD benchmark, ranking **first** on 11 datasets for MSE and 10 for MAE. This underscores its strong ability to capture complex inter-channel dependencies by learning hierarchical latent channel structures compared to other CD models. In contrast, iTransformer, the representative CD model that explicitly models multivariate correlations via Transformer, underperforms on many datasets. This may be due to the extreme complexity of channel dependencies in a high-dimensional

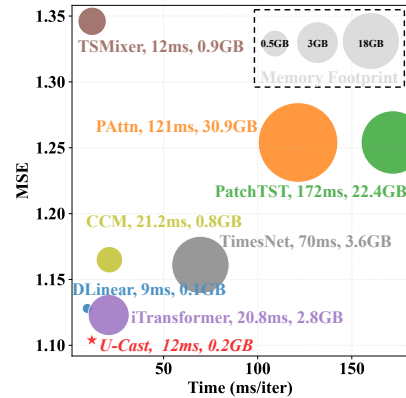


Figure 3: MSE vs. average training time per batch on Wind dataset ($C = 3,850$); marker size reflects GPU memory usage.

setting, where the lack of an explicitly hierarchical structure learning in its attention mechanism limits its effectiveness. By explicitly learning latent hierarchical structure by hierarchical latent query and full-rank regularization, U-CAST is better equipped to handle such complexity.

Model Efficiency. Beyond its strong forecasting performance, another notable advantage of U-CAST is its lightweight architecture. Figure 3 shows U-CAST achieves the best trade-off between training speed, memory footprint, and performance. We also find that U-CAST consistently achieves favorable training efficiency across varying dimensionalities and as dimensionality increases, the efficiency advantage of U-CAST over other methods becomes more pronounced (see Appendix O). Additionally, we conduct computational complexity analysis, which indicates that U-CAST lowers both time and memory by a factor of r compared with iTransformer, yet still retains the expressive power of attention through its latent-query hierarchy (see Appendix J).

Ablation Study. We evaluate the impact of: (1) **w/o hierarchical** by retaining only a single layer for dimensionality reduction, (2) **w/o latent query** by setting Q_ℓ requires_grad=False, and (3) **w/o upsampling** by using a simple linear projection to restore channel dimension. In addition, we examine the role of the covariance full-rank regularization by **w/o \mathcal{L}_{cov}** , i.e., setting $\alpha = 0$. Table 4 shows that removing any component degrades U-CAST’s averaged performance, confirming their necessity. For the full results on all datasets and deeper analysis, we refer reader to Appendix P.

Table 4: Ablation study on different components of U-CAST. The results are averaged over 16 datasets, with the complete results provided in Table 7.

Variant	MSE	MAE
U-CAST	1.243	0.326
w/o \mathcal{L}_{cov}	1.267	0.341
w/o Hierarchical	1.263	0.332
w/o Latent Query	1.260	0.331
w/o Upsampling	1.269	0.336

Does full-rank regularization \mathcal{L}_{cov} disentangle channels correlation effectively? As shown in Figure 4 (a), the top four subplots visualize the evolution of the covariance matrix Σ from a randomly initialized state (Epoch 0) to a well-optimized one (Epoch 10). The structure of the covariance matrix changes significantly across epochs, transitioning from dense to more sparse. This indicates that \mathcal{L}_{cov} is effectively promoting disentanglement by reducing redundancy among channels.

Can U-CAST learn latent hierarchical structure among channels?

As shown in Figure 4 (b), we visualize the attention maps at different layers. The attention focuses vary across layers, reflecting a latent hierarchical structure in the learned representations. Furthermore, assigning dimension reduction and multivariate correlation modeling to the attention mechanism improves the interpretability of attention maps. Figure 4 (c) shows attention maps from the hierarchical latent query network on the Measles dataset ($C = 1161, 387$ regions \times 3 features: **I**-Inferred Infections, **P**-Population, **S**-Suspected Cases). Five regions are selected (colors indicate regions). At $L = 1$, the model reduces to $C_1 = 32$ latent dimensions (visualizing 19–24), and at $L = 2$, to $C_2 = 8$. At $L = 1$, dimensions 19–22 mainly attend to P and S, while 23–24 focus on I. At $L = 2$, dimensions 1–4 attend to outputs from 19–22, and 5–8 to those from 23–24. This pattern reflects a learned hierarchy: the model first separates features within regions, then integrates related features across regions, revealing a meaningful latent channel structure.

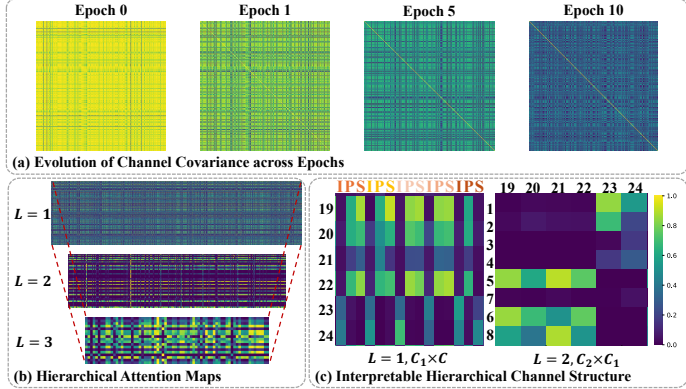


Figure 4: A showcase on Measles dataset of full-rank regularization and latent hierarchical channel structure learning.

7 Conclusion and Future Opportunities

In this paper, we propose U-CAST to address the unique challenges of effectively modeling these latent hierarchical channel structures within High-Dimensional Time Series Forecasting (HDTSF). To facilitate research in HDTSF and provide a testbed for U-CAST and future innovative approaches,

we curate the TIME-HD benchmark. Through extensive experiments using our new benchmark, we identify and highlight key research directions and opportunities within high-dimensional time series forecasting: (1) scalable modeling for high-dimensional time series forecasting, (2) enhanced inter-channel correlation learning, and (3) standardized benchmarking protocols. It is our aspiration that U-CAST, TIME-HD, and their accompanying resources will serve as a significant catalyst for innovation and progress in the field.

References

- [1] Abdul Fatir Ansari, Lorenzo Stella, Caner Turkmen, Xiyuan Zhang, Pedro Mercado, Huibin Shen, Oleksandr Shchur, Syama Sundar Rangapuram, Sebastian Pineda Arango, Shubham Kapoor, et al. Chronos: Learning the language of time series. *arXiv preprint arXiv:2403.07815*, 2024.
- [2] André Bauer, Marwin Züfle, Simon Eismann, Johannes Grohmann, Nikolas Herbst, and Samuel Kounev. Libra: A benchmark for time series forecasting methods. In *Proceedings of the ACM/SPEC International Conference on Performance Engineering*, pages 189–200, 2021.
- [3] Yongli Cai, Yun Kang, Malay Banerjee, and Weiming Wang. A stochastic sirs epidemic model with infectious force under intervention strategies. *Journal of Differential Equations*, 259(12):7463–7502, 2015.
- [4] Caglar Cakan, Nikola Jajcay, and Klaus Obermayer. neurolib: A simulation framework for whole-brain neural mass modeling. *Cognitive Computation*, Oct 2021.
- [5] Chris Chatfield. *Time-series forecasting*. Chapman and Hall/CRC, 2000.
- [6] Jialin Chen, Jan Eric Lenssen, Aosong Feng, Weihua Hu, Matthias Fey, Leandros Tassiulas, Jure Leskovec, and Rex Ying. From similarity to superiority: Channel clustering for time series forecasting. *Advances in Neural Information Processing Systems*, 37:130635–130663, 2024.
- [7] Si-An Chen, Chun-Liang Li, Nate Yoder, Sercan O Arik, and Tomas Pfister. Tsmixer: An all-mlp architecture for time series forecasting. *arXiv preprint arXiv:2303.06053*, 2023.
- [8] Israel Cohen, Yiteng Huang, Jingdong Chen, Jacob Benesty, Jacob Benesty, Jingdong Chen, Yiteng Huang, and Israel Cohen. Pearson correlation coefficient. *Noise reduction in speech processing*, pages 1–4, 2009.
- [9] Cameron Craddock, Yassine Benhajali, Carlton Chu, Francois Chouinard, Alan Evans, Andrés Jakab, Budhachandra Singh Khundrakpam, John David Lewis, Qingyang Li, Michael Milham, et al. The neuro bureau preprocessing initiative: open sharing of preprocessed neuroimaging data and derivatives. *Frontiers in Neuroinformatics*, 7(27):5, 2013.
- [10] Tao Dai, Beiliang Wu, Peiyuan Liu, Naiqi Li, Jigang Bao, Yong Jiang, and Shu-Tao Xia. Periodicity decoupling framework for long-term series forecasting. In *The Twelfth International Conference on Learning Representations*, 2024.
- [11] Abhimanyu Das, Weihao Kong, Rajat Sen, and Yichen Zhou. A decoder-only foundation model for time-series forecasting. In *Forty-first International Conference on Machine Learning*, 2024.
- [12] Jan G De Gooijer and Rob J Hyndman. 25 years of time series forecasting. *International journal of forecasting*, 22(3):443–473, 2006.
- [13] Tianning Feng, Juntong Ni, Ezequiel Gleichgerricht, and Wei Jin. Seizureformer: A transformer model for ica-based seizure risk forecasting. *arXiv preprint arXiv:2504.16098*, 2025.
- [14] Rakshitha Godahewa, Christoph Bergmeir, Geoffrey I Webb, Rob J Hyndman, and Pablo Montero-Manso. Monash time series forecasting archive. *arXiv preprint arXiv:2105.06643*, 2021.
- [15] Google. Google covid-19 community mobility reports, 2020. Accessed: <date>.
- [16] Mononito Goswami, Konrad Szafer, Arjun Choudhry, Yifu Cai, Shuo Li, and Artur Dubrawski. Moment: A family of open time-series foundation models. *arXiv preprint arXiv:2402.03885*, 2024.
- [17] Clive William John Granger and Paul Newbold. *Forecasting economic time series*. Academic press, 2014.
- [18] Addison Howard, inversion, Spyros Makridakis, and vangelis. M5 forecasting - accuracy. <https://kaggle.com/competitions/m5-forecasting-accuracy>, 2020. Kaggle.

- [19] Diederik P Kingma and Jimmy Ba. Adam: A method for stochastic optimization. *arXiv preprint arXiv:1412.6980*, 2014.
- [20] Guokun Lai, Wei-Cheng Chang, Yiming Yang, and Hanxiao Liu. Modeling long-and short-term temporal patterns with deep neural networks. In *The 41st international ACM SIGIR conference on research & development in information retrieval*, pages 95–104, 2018.
- [21] Yubo Liang, Zezhi Shao, Fei Wang, Zhao Zhang, Tao Sun, and Yongjun Xu. Basicts: An open source fair multivariate time series prediction benchmark. In *International symposium on benchmarking, measuring and optimization*, pages 87–101. Springer, 2022.
- [22] Bryan Lim and Stefan Zohren. Time-series forecasting with deep learning: a survey. *Philosophical Transactions of the Royal Society A*, 379(2194):20200209, 2021.
- [23] Shengsheng Lin, Weiwei Lin, Wentai Wu, Haojun Chen, and Junjie Yang. Sparsetsf: Modeling long-term time series forecasting with 1k parameters. *arXiv preprint arXiv:2405.00946*, 2024.
- [24] Xu Liu, Yutong Xia, Yuxuan Liang, Junfeng Hu, Yiwei Wang, Lei Bai, Chao Huang, Zhenguang Liu, Bryan Hooi, and Roger Zimmermann. Largest: A benchmark dataset for large-scale traffic forecasting. *Advances in Neural Information Processing Systems*, 36:75354–75371, 2023.
- [25] Yong Liu, Tengge Hu, Haoran Zhang, Haixu Wu, Shiyu Wang, Lintao Ma, and Mingsheng Long. itransformer: Inverted transformers are effective for time series forecasting. In *The Twelfth International Conference on Learning Representations*, 2024.
- [26] Yong Liu, Haixu Wu, Jianmin Wang, and Mingsheng Long. Non-stationary transformers: Exploring the stationarity in time series forecasting. *Advances in neural information processing systems*, 35:9881–9893, 2022.
- [27] Zewen Liu, Yunxiao Li, Mingyang Wei, Guancheng Wan, Max SY Lau, and Wei Jin. Epilearn: A python library for machine learning in epidemic modeling. *arXiv preprint arXiv:2406.06016*, 2024.
- [28] Zewen Liu, Juntong Ni, Max SY Lau, and Wei Jin. Cape: Covariate-adjusted pre-training for epidemic time series forecasting. *arXiv preprint arXiv:2502.03393*, 2025.
- [29] Carl H Lubba, Sarab S Sethi, Philip Knaute, Simon R Schultz, Ben D Fulcher, and Nick S Jones. catch22: Canonical time-series characteristics: Selected through highly comparative time-series analysis. *Data mining and knowledge discovery*, 33(6):1821–1852, 2019.
- [30] Donghao Luo and Xue Wang. Modernctn: A modern pure convolution structure for general time series analysis. In *The Twelfth International Conference on Learning Representations*, 2024.
- [31] Wyatt G Madden, Wei Jin, Benjamin Lopman, Andreas Zufle, Benjamin Dalziel, C Jessica E. Metcalf, Bryan T Grenfell, and Max SY Lau. Deep neural networks for endemic measles dynamics: Comparative analysis and integration with mechanistic models. *PLOS Computational Biology*, 20(11):e1012616, 2024.
- [32] Spyros Makridakis and Michele Hibon. The m3-competition: results, conclusions and implications. *International journal of forecasting*, 16(4):451–476, 2000.
- [33] Spyros Makridakis, Evangelos Spiliotis, and Vassilios Assimakopoulos. The m4 competition: Results, findings, conclusion and way forward. *International Journal of forecasting*, 34(4):802–808, 2018.
- [34] Juntong Ni, Zewen Liu, Shiyu Wang, Ming Jin, and Wei Jin. Timedistill: Efficient long-term time series forecasting with mlp via cross-architecture distillation. *arXiv preprint arXiv:2502.15016*, 2025.
- [35] Yuqi Nie, Nam H Nguyen, Phanwadee Sinthong, and Jayant Kalagnanam. A time series is worth 64 words: Long-term forecasting with transformers. In *The Eleventh International Conference on Learning Representations*, 2023.

- [36] Boris N. Oreshkin, Dmitri Carпов, Nicolas Chapados, and Yoshua Bengio. N-beats: Neural basis expansion analysis for interpretable time series forecasting. In *International Conference on Learning Representations*, 2020.
- [37] A Paszke. Pytorch: An imperative style, high-performance deep learning library. *arXiv preprint arXiv:1912.01703*, 2019.
- [38] Xiangfei Qiu, Jilin Hu, Lekui Zhou, Xingjian Wu, Junyang Du, Buang Zhang, Chenjuan Guo, Aoying Zhou, Christian S Jensen, Zhenli Sheng, et al. Tfb: Towards comprehensive and fair benchmarking of time series forecasting methods. *arXiv preprint arXiv:2403.20150*, 2024.
- [39] Xiangfei Qiu, Xingjian Wu, Yan Lin, Chenjuan Guo, Jilin Hu, and Bin Yang. Duet: Dual clustering enhanced multivariate time series forecasting. *arXiv preprint arXiv:2412.10859*, 2024.
- [40] Xiaoming Shi, Shiyu Wang, Yuqi Nie, Dianqi Li, Zhou Ye, Qingsong Wen, and Ming Jin. Time-moe: Billion-scale time series foundation models with mixture of experts. *arXiv preprint arXiv:2409.16040*, 2024.
- [41] James H Stock and Mark W Watson. Vector autoregressions. *Journal of Economic perspectives*, 15(4):101–115, 2001.
- [42] Mingtian Tan, Mike Merrill, Vinayak Gupta, Tim Althoff, and Tom Hartvigsen. Are language models actually useful for time series forecasting? *Advances in Neural Information Processing Systems*, 37:60162–60191, 2024.
- [43] Can Wan, Jian Zhao, Yonghua Song, Zhao Xu, Jin Lin, and Zechun Hu. Photovoltaic and solar power forecasting for smart grid energy management. *CSEE Journal of power and energy systems*, 1(4):38–46, 2015.
- [44] Shiyu Wang, Haixu Wu, Xiaoming Shi, Tengge Hu, Huakun Luo, Lintao Ma, James Y Zhang, and Jun Zhou. Timemixer: Decomposable multiscale mixing for time series forecasting. *arXiv preprint arXiv:2405.14616*, 2024.
- [45] Yuxuan Wang, Haixu Wu, Jiaxiang Dong, Yong Liu, Mingsheng Long, and Jianmin Wang. Deep time series models: A comprehensive survey and benchmark. *arXiv preprint arXiv:2407.13278*, 2024.
- [46] Yuxuan Wang, Haixu Wu, Jiaxiang Dong, Guo Qin, Haoran Zhang, Yong Liu, Yunzhong Qiu, Jianmin Wang, and Mingsheng Long. Timexer: Empowering transformers for time series forecasting with exogenous variables. *arXiv preprint arXiv:2402.19072*, 2024.
- [47] Gerald Woo, Chenghao Liu, Akshat Kumar, Caiming Xiong, Silvio Savarese, and Doyen Sahoo. Unified training of universal time series forecasting transformers. 2024.
- [48] Haixu Wu, Tengge Hu, Yong Liu, Hang Zhou, Jianmin Wang, and Mingsheng Long. Timesnet: Temporal 2d-variation modeling for general time series analysis. *arXiv preprint arXiv:2210.02186*, 2022.
- [49] Haixu Wu, Jiehui Xu, Jianmin Wang, and Mingsheng Long. Autoformer: Decomposition transformers with auto-correlation for long-term series forecasting. *Advances in neural information processing systems*, 34:22419–22430, 2021.
- [50] Haixu Wu, Hang Zhou, Mingsheng Long, and Jianmin Wang. Interpretable weather forecasting for worldwide stations with a unified deep model. *Nature Machine Intelligence*, 5(6):602–611, 2023.
- [51] Zhijian Xu, Ailing Zeng, and Qiang Xu. Fits: Modeling time series with 10k parameters. *arXiv preprint arXiv:2307.03756*, 2023.
- [52] Xueyan Yin, Genze Wu, Jinze Wei, Yanming Shen, Heng Qi, and Baocai Yin. Deep learning on traffic prediction: Methods, analysis, and future directions. *IEEE Transactions on Intelligent Transportation Systems*, 23(6):4927–4943, 2021.

- [53] Ailing Zeng, Muxi Chen, Lei Zhang, and Qiang Xu. Are transformers effective for time series forecasting? In *Proceedings of the AAAI conference on artificial intelligence*, volume 37, pages 11121–11128, 2023.
- [54] Yunhao Zhang and Junchi Yan. Crossformer: Transformer utilizing cross-dimension dependency for multivariate time series forecasting. In *The Eleventh International Conference on Learning Representations*, 2023.
- [55] Lifan Zhao and Yanyan Shen. Rethinking channel dependence for multivariate time series forecasting: Learning from leading indicators. *arXiv preprint arXiv:2401.17548*, 2024.
- [56] Zhiyuan Zhao, Juntong Ni, Shangqing Xu, Haoxin Liu, Wei Jin, and B Aditya Prakash. Timerecipe: A time-series forecasting recipe via benchmarking module level effectiveness. *arXiv preprint arXiv:2506.06482*, 2025.
- [57] Zhiyuan Zhao, Sitan Yang, Kin G Olivares, Boris N Oreshkin, Stan Vitebsky, Michael W Mahoney, B Aditya Prakash, and Dmitry Efimov. Tat: Temporal-aligned transformer for multi-horizon peak demand forecasting. *arXiv preprint arXiv:2507.10349*, 2025.
- [58] Haoyi Zhou, Shanghang Zhang, Jieqi Peng, Shuai Zhang, Jianxin Li, Hui Xiong, and Wancai Zhang. Informer: Beyond efficient transformer for long sequence time-series forecasting. In *Proceedings of the AAAI conference on artificial intelligence*, volume 35, pages 11106–11115, 2021.
- [59] Tian Zhou, Ziqing Ma, Qingsong Wen, Xue Wang, Liang Sun, and Rong Jin. Fedformer: Frequency enhanced decomposed transformer for long-term series forecasting. In *International conference on machine learning*, pages 27268–27286. PMLR, 2022.

A Comparison with Existing Works

Property	Multivariate	High-Dimensional (≥ 1000)	Temporal Alignment	Evaluation
Benchmark				
M3 [32]	✗	✗	✗	✗
M4 [33]	✗	✗	✗	✗
LTSF-Linear [53]	✓	✗	✓	✗
TSlib [48]	✓	✗	✓	✗
BasicTS [21]	✓	✗	✓	✗
BasicTS+ [21]	✓	✗	✓	✗
Monash [14]	✗	✗	✗	✗
Libra [2]	✗	✗	✗	✗
TFB [38]	✓	✓ (only one)	✓ (only one)	✓ (only one)
Foundation Models				
Chronos [1]	✓	✓	✗	✗
Moment [16]	✓	✓	✗	✗
Moirai [47]	✓	✓	✗	✗
TimesFM [11]	✓	✓	✗	✗
Time-MoE [40]	✓	✓ (only one)	✓ (only one)	✓ (only one)
Ours				
TIME-HD	✓	✓	✓	✓

Table 5: Comparison of datasets in benchmarks and foundation models on four properties: (1) **Multivariate** indicates whether the datasets involve multiple variables (more than one channel). (2) **High-Dimensional (≥ 1000)** refers to the presence of datasets with at least 1000 channels, either for pretraining or evaluation. (3) **Temporal Alignment** denotes whether the datasets are temporally aligned. (4) **Evaluation** assesses whether high-dimensional datasets are used specifically for evaluation purposes.

High-Dimensional Time Series Datasets. As shown in Table 5, most existing benchmarks do not include any high-dimensional datasets. The only exception is TFB [38], which incorporates only one dataset with 2000 channels (Wiki2000) for evaluation. Among foundation models, although all of them include high-dimensional time series datasets, these datasets are primarily used for pretraining rather than evaluation. Time-MoE [40] is the only one that evaluates on a high-dimensional dataset (Global Temp) with 1000 channels. Both TFB and Time-MoE attempt to explore the high-dimensional regime, but they each include **only one** such dataset. This limited coverage constrains their effectiveness as comprehensive benchmarks.

Multivariate Time Series Forecasting. *Channel-independent (CI):* The CI modeling strategy uses a shared model backbone for all channels and processes each channel independently during the forward pass [35, 53, 51, 44, 42, 10, 23]. This design generally results in lower model capacity but offers greater robustness. However, since CI models treat each channel independently, they are unable to capture inter-channel correlations explicitly.

Channel-dependent (CD): In contrast, the CD modeling strategy incorporates modules that are specifically designed to capture dependencies across channels. These methods tend to offer higher model capacity and can leverage cross-channel information more effectively. Based on how the inter-channel correlations are handled, CD approaches can be categorized as follows: (1) Position-wise [7, 48, 49, 58, 59, 54]: These methods first project the channel dimension of each time step into a hidden embedding space, resulting in one embedding per time step. This approach may ignore correlations across channels at different time steps and could introduce noise. After generating the embeddings, these methods mainly focus on modeling temporal dependencies. (2) Token-wise [25, 46]: These methods treat each channel as a token and input the sequence of tokens into a Transformer model. This helps reduce irrelevant noise for forecasting. Although multi-layer Transformers have the potential to capture complex hierarchical inter-channel structures, they are extremely time-consuming and do not scale well to high-dimensional time series. Moreover, the lack of an explicit mechanism for learning hierarchical channel structure may limit their effectiveness. (3) Cluster-wise [6, 39]: These approaches divide the multivariate time series into disjoint channel clusters using clustering algorithms. However, using a single-layer clustering step may overlook the hierarchical organization present in high-dimensional time series, which can lead to suboptimal performance.

B Future Opportunity

Scaling Forecasting Models to High-Dimensional Time Series. Most existing forecasting models are developed and benchmarked on low-dimensional datasets, which restricts their practical relevance in high-dimensional applications. As the number of variables increases, computational and memory bottlenecks become more prominent, especially for models employing attention mechanisms or dense channel-wise operations. Future research can prioritize the development of architectures that maintain accuracy while achieving sub-quadratic complexity in the number of channels. In particular, scalable attention mechanisms, parameter-efficient representations, and adaptive channel selection strategies are promising directions.

Improving the Ability of Models to Capture Inter-Channel Correlations. High-dimensional time series often exhibit rich and structured inter-channel dependencies, including spatial, semantic, and hierarchical patterns. While U-CAST demonstrates that learning latent hierarchical structures can be effective, there remains room to improve in two aspects: (1) dynamic correlation modeling that adapts to temporal shifts in inter-variable relationships, and (2) domain-aware inductive biases that can leverage prior knowledge (e.g., spatial topology, sectoral information) to guide the learning of channel relationships. Better capturing these correlations can lead to models that are both more interpretable and more robust to distributional changes.

Benchmarking and Standardization for High-Dimensional Forecasting. Despite the introduction of the TIME-HD benchmark, the evaluation of forecasting models in high-dimensional regimes remains underdeveloped. Future work should explore more comprehensive evaluation protocols, including robustness to missing channels, adaptation to distribution drift, and generalization to unseen domains. Additionally, standardized metrics for scalability and memory efficiency, beyond predictive accuracy, are needed to holistically compare models in real-world deployment scenarios.

C Limitations

First, U-CAST still needs attention to capture channel correlation, which incurs high computational cost although it has already achieved superior efficiency compared to other baselines. **Second**, the number of layers and the reduction ratio need to be predefined, which may limit its utilization across datasets with varying hierarchical complexity and scale. **Third**, the effectiveness of U-CAST relies on the presence of strong latent hierarchical structures in the data. In datasets where inter-channel dependencies are weak, sparse, or not semantically organized, the performance advantage may diminish. Furthermore, the model assumes that these structures are learnable through attention and full-rank regularization, but this may not hold in scenarios with extremely noisy or low-signal input features, leading to suboptimal disentanglement and degraded forecasting accuracy.

D Social Impact

Transparency Impact. Transparency is essential for promoting accountability, enabling fair comparison, and advancing collective understanding. To support these goals, we will publicly release our codebase, datasets, and evaluation pipeline. However, in accordance with anonymized submission requirements, these materials are currently provided only in the supplementary material.

Environmental Impact. U-CAST offers efficient inference, which reduces GPU runtime and, consequently, the overall energy consumption. This efficiency helps lower the associated carbon emissions, particularly from energy-intensive local power grids.

Ethical Impact. Although U-CAST shows strong performance in high-dimensional time series forecasting, its deployment in critical domains such as healthcare requires caution. In high-stakes settings, inaccurate forecasts could lead to harmful outcomes, underscoring the importance of thorough validation and domain-specific safeguards.

E Theorem 1 Proof

Proof. Our goal is to forecast $z_t = \begin{pmatrix} z_t^{(1)} \\ z_t^{(2)} \end{pmatrix}$. For simplicity, we focus on forecasting $z_{t+1}^{(1)}$; forecasting $z_{t+1}^{(2)}$ is analogous. In a single forward process, the CI forecaster observes only $x = z_t^{(1)}$ and does **not** observe $w = z_t^{(2)}$. The optimal forecast under squared-error loss is the conditional expectation $\mathbb{E}[z_{t+1}^{(1)} | x]$. From the Equation 1, $z_{t+1}^{(i)} = a_{11}x + a_{12}w + \varepsilon$, where $\varepsilon = \varepsilon_{t+1}^{(1)} \sim \mathcal{N}(0, \sigma_{11})$. The conditional distribution of w given x is Gaussian. The optimal forecast is:

$$\mathbb{E}[z_{t+1}^{(1)} | x] = \mathbb{E}[a_{11}x + a_{12}w + \varepsilon | x] = a_{11}x + a_{12}\mathbb{E}[w | x] + \mathbb{E}[\varepsilon | x].$$

Since ε is independent of x (and w), $\mathbb{E}[\varepsilon | x] = \mathbb{E}[\varepsilon] = 0$ (as ε has zero mean). Thus,

$$\mathbb{E}[z_{t+1}^{(1)} | x] = a_{11}x + a_{12}\mathbb{E}[w | x].$$

The CI Bayes risk is the expected squared error of this optimal forecast:

$$\begin{aligned} R_{\text{CI}} &= \mathbb{E}[(z_{t+1}^{(1)} - \mathbb{E}[z_{t+1}^{(1)} | x])^2] \\ &= \mathbb{E}[(a_{11}x + a_{12}w + \varepsilon - (a_{11}x + a_{12}\mathbb{E}[w | x]))^2] \\ &= \mathbb{E}[(a_{12}(w - \mathbb{E}[w | x]) + \varepsilon)^2] \\ &= \mathbb{E}[a_{12}^2(w - \mathbb{E}[w | x])^2] + \mathbb{E}[\varepsilon^2] + 2a_{12}\mathbb{E}[(w - \mathbb{E}[w | x])\varepsilon]. \end{aligned}$$

Again, using the independence of ε from w and x (and thus from $\mathbb{E}[w | x]$), the cross-term expectation is zero: $\mathbb{E}[(w - \mathbb{E}[w | x])\varepsilon] = \mathbb{E}[w - \mathbb{E}[w | x]]\mathbb{E}[\varepsilon] = 0$. The first term is a_{12}^2 times the definition of the conditional variance, $\text{Var}(w | x) = \mathbb{E}[(w - \mathbb{E}[w | x])^2]$, since w has zero mean (due to normalization) and $\mathbb{E}[w | x]$ is the conditional mean. Therefore,

$$\begin{aligned} R_{\text{CI}} &= a_{12}^2 \text{Var}(w | x) + \mathbb{E}[\varepsilon^2] \\ &= \sigma_{11} + a_{12}^2 \text{Var}(w | x). \end{aligned}$$

Note that our assumption that the time series are normalized (zero mean) simplifies the interpretation but the structure of the result holds more generally.

In a single forward process, the CD forecaster observes **both** $x = z_t^{(1)}$ and $w = z_t^{(2)}$. The optimal forecast is $\mathbb{E}[z_{t+1}^{(1)} | x, w]$.

$$\mathbb{E}[z_{t+1}^{(1)} | x, w] = \mathbb{E}[a_{11}x + a_{12}w + \varepsilon | x, w] = a_{11}x + a_{12}w + \mathbb{E}[\varepsilon | x, w].$$

Since $\varepsilon = \varepsilon_{t+1}^{(1)}$ is independent of both $x = z_t^{(1)}$ and $w = z_t^{(2)}$, $\mathbb{E}[\varepsilon | x, w] = \mathbb{E}[\varepsilon] = 0$. Thus,

$$\mathbb{E}[z_{t+1}^{(1)} | x, w] = a_{11}x + a_{12}w.$$

The CD Bayes risk is:

$$\begin{aligned} R_{\text{CD}} &= \mathbb{E}[(Y - \mathbb{E}[z_{t+1}^{(1)} | x, w])^2] \\ &= \mathbb{E}[(a_{11}x + a_{12}w + \varepsilon - (a_{11}x + a_{12}w))^2] \\ &= \mathbb{E}[\varepsilon^2] = \sigma_{11}. \end{aligned}$$

Comparing the two risks, we see that the reduction in risk from using the CD compared to the CI one is:

$$R_{\text{CI}} - R_{\text{CD}} = (\sigma_{11} + a_{12}^2 \text{Var}(w | x)) - \sigma_{11} = a_{12}^2 \text{Var}(w | x).$$

This difference is non-negative since $a_{12}^2 \geq 0$ and the conditional variance $\text{Var}(w | x) \geq 0$. The risk reduction is strictly positive if $a_{12} \neq 0$ and $\text{Var}(w | x) > 0$. This occurs when the second channel (w) has a non-zero direct influence on the first channel in the next period ($a_{12} \neq 0$) and when the second channel carries some information not already present in the first channel (i.e., w is not perfectly predictable from x , ensuring $\text{Var}(w | x) > 0$). If $a_{12} = 0$, or if w is perfectly predictable from x , the risks are equal. Similarly, if we focus on forecasting $z_{t+1}^{(2)}$, we have:

$$R_{\text{CI}} - R_{\text{CD}} = (\sigma_{22} + a_{21}^2 \text{Var}(w | x)) - \sigma_{22} = a_{21}^2 \text{Var}(w | x).$$

Thus, $\sum_i^2 (R_{\text{CI}} - R_{\text{CD}}) = a_{12}^2 \text{Var}(w | x) + a_{21}^2 \text{Var}(x | w) > 0$. This example demonstrates that, under squared-error loss for a linear Gaussian VAR model, using the CD leads to a Bayes risk that is always less than or equal to the Bayes risk obtained using only the CI.

□

F Theorem 2 Proof

Proof. Let $\mathcal{F}_p = \sigma(z_t^{(1)}, \dots, z_t^{(p)})$ denote the sigma-field generated by the first p channels at time t . The Bayes risk under squared-error loss using information set \mathcal{F}_p is:

$$R_p = \mathbb{E} [(Y - \mathbb{E}[Y | \mathcal{F}_p])^2].$$

Since conditional expectation minimizes mean squared error, and since the information sets are nested ($\mathcal{F}_1 \subseteq \dots \subseteq \mathcal{F}_P$), we have:

$$R_1 \geq R_2 \geq \dots \geq R_P = \mathbb{E}[(\varepsilon_{t+1}^{(1)})^2] = \sigma_{11},$$

where the last equality holds because \mathcal{F}_P fully determines the conditional mean of Y , and the only uncertainty is from the innovation $\varepsilon_{t+1}^{(1)}$.

Define the risk reduction relative to the univariate forecast as:

$$\Delta_p = R_1 - R_p.$$

The monotonicity of R_p implies that Δ_p is non-decreasing:

$$0 = \Delta_1 \leq \Delta_2 \leq \dots \leq \Delta_P = R_1 - \sigma_{11}.$$

To characterize when the inequality is strict, note that $\Delta_p > \Delta_{p-1}$ if and only if:

$$R_p < R_{p-1}.$$

This occurs if the p -th channel $z_t^{(p)}$ provides additional information about Y beyond what is already available from $z_t^{(1)}, \dots, z_t^{(p-1)}$. In the VAR(1) context, this requires:

- $a_{1p} \neq 0$, so that $z_t^{(p)}$ directly affects Y ;
- $\text{Var}(z_t^{(p)} | z_t^{(1)}, \dots, z_t^{(p-1)}) > 0$, so that $z_t^{(p)}$ is not a deterministic function of the previous channels.

If either condition fails, then $z_t^{(p)}$ does not improve the forecast of Y , and $R_p = R_{p-1}$. Therefore, each strictly decreasing step in Bayes risk corresponds to the inclusion of a new, informative, and non-redundant channel. □

G Theorem 3 Proof

Proof. Write the compact singular-value decomposition of $\mathbf{H}^{(\ell-1)}$ as $\mathbf{H}^{(\ell-1)} = \mathbf{U} \mathbf{\Sigma} \mathbf{V}^\top$, where $\mathbf{U} \in \mathbb{R}^{C \times r}$, $\mathbf{\Sigma} \in \mathbb{R}^{r \times r}$ is diagonal with positive entries, $\mathbf{V} \in \mathbb{R}^{d \times r}$, and the columns of \mathbf{U} form an orthonormal basis of the row-space of $\mathbf{H}^{(\ell-1)}$. Because $r \geq C'$ by assumption, we can pick a matrix $\mathbf{Q} \in \mathbb{R}^{C' \times C}$ of full row rank whose rows are any C' independent linear combinations of the rows of \mathbf{U}^\top . Formally, let $\mathbf{S} \in \mathbb{R}^{C' \times C}$ select those C' rows (so $\mathbf{S}\mathbf{S}^\top = \mathbf{I}_{C'}$), and set $\mathbf{Q} = \mathbf{S}$. Then

$$\mathbf{H}^{(\ell)} = \mathbf{Q}\mathbf{H}^{(\ell-1)} = \mathbf{S}\mathbf{U} \mathbf{\Sigma} \mathbf{V}^\top.$$

Since $\mathbf{S}\mathbf{U} \in \mathbb{R}^{C' \times r}$ has full row rank C' ,

$$\text{rank}(\mathbf{H}^{(\ell)}) = \text{rank}(\mathbf{S}\mathbf{U}) = C',$$

which proves the first claim. Assume further that $r \geq d$ and $C' \geq d$, so the maximal attainable row rank is d . Define $\mathbf{\Sigma}^{(\ell)} = \frac{1}{d} \mathbf{H}^{(\ell)} \mathbf{H}^{(\ell)\top} \in \mathbb{R}^{C' \times C'}$. Adding the penalty $\mathcal{L}_{\text{cov}} = -\frac{1}{C'} \log \det(\mathbf{\Sigma}^{(\ell)} + \varepsilon \mathbf{I}_{C'})$ in training maximises $\det(\mathbf{\Sigma}^{(\ell)}) = \prod_{i=1}^{C'} \sigma_i^2$, where σ_i are the singular values of $\mathbf{H}^{(\ell)}$. Because the product of the singular values grows when any σ_i that is near zero increases, gradient descent on $-\log \det(\cdot)$ pushes all σ_i away from zero, thereby driving $\mathbf{H}^{(\ell)}$ toward full row rank $\min(C', d)$.

Compatibility with HLQN attention. In HLQN the ℓ -th block produces $\mathbf{H}^{(\ell)} = W_o(\text{softmax}(W_q \mathbf{Q}_\ell (W_k \mathbf{H}^{(\ell-1)})^\top / \sqrt{d_h}) W_v \mathbf{H}^{(\ell-1)})$. Write the attention weights as $\mathbf{A}(\mathbf{H}^{(\ell-1)}) = \text{softmax}(W_q \mathbf{Q}_\ell (W_k \mathbf{H}^{(\ell-1)})^\top / \sqrt{d_h}) \in \mathbb{R}^{C_\ell \times C}$. Then

$$\mathbf{H}^{(\ell)} = \underbrace{W_o \mathbf{A}(\mathbf{H}^{(\ell-1)}) W_v}_{\mathbf{Q}(\mathbf{H}^{(\ell-1)})} \mathbf{H}^{(\ell-1)}.$$

$\mathbf{Q}(\mathbf{H}^{(\ell-1)}) \in \mathbb{R}^{C_\ell \times C}$

Hence each forward pass is algebraically identical to left-multiplying $\mathbf{H}^{(\ell-1)}$ by a sample-dependent matrix $\mathbf{Q}(\mathbf{H}^{(\ell-1)})$. As long as $\mathbf{Q}(\mathbf{H}^{(\ell-1)})$ has full row rank C_ℓ —a property encouraged by the LogDet regulariser—the rank analysis above applies verbatim: $\text{rank}(\mathbf{H}^{(\ell)}) = C_\ell$ and the gradient of the regulariser still pushes every singular value of $\mathbf{H}^{(\ell)}$ away from zero. Therefore the conclusions of Theorem 3 remain valid for the Hierarchical Latent Query Network attention block. \square

H Theorem of Information Reduction

Theorem 4 (Entropy Monotonicity of the Covariance Loss). *Assume the rows of $\mathbf{H}^{(\ell)} \in \mathbb{R}^{C' \times d}$ follow an i.i.d. zero-mean Gaussian distribution $\mathcal{N}(\mathbf{0}, \Sigma^{(\ell)})$ with $\Sigma^{(\ell)} = \frac{1}{d} \mathbf{H}^{(\ell)} \mathbf{H}^{(\ell)\top} \succ \mathbf{0}$. Define the differential entropy*

$$h^{(\ell)} = \frac{1}{2} \log\left((2\pi e)^{C'} \det(\Sigma^{(\ell)})\right).$$

Let

$$\mathcal{L}_{\text{cov}}^{(\ell)} = -\frac{1}{C'} \log \det(\Sigma^{(\ell)} + \varepsilon I_{C'}), \quad \varepsilon > 0.$$

Then, along any differentiable optimisation trajectory $t \mapsto \mathbf{H}^{(\ell)}(t)$ that decreases $\mathcal{L}_{\text{cov}}^{(\ell)}$, the entropy satisfies

$$\frac{d}{dt} h^{(\ell)}(t) = -\frac{C'}{2} \frac{d}{dt} \mathcal{L}_{\text{cov}}^{(\ell)}(t) \geq 0,$$

with equality if and only if $\nabla_{\mathbf{H}^{(\ell)}} \mathcal{L}_{\text{cov}}^{(\ell)} = \mathbf{0}$. Hence every strict descent step on $\mathcal{L}_{\text{cov}}^{(\ell)}$ strictly increases the Shannon differential entropy of the latent channel distribution.

Proof. For brevity drop the layer index (ℓ) and write $\Sigma = \Sigma^{(\ell)}(t)$. Since $\Sigma \succ \mathbf{0}$ and $\varepsilon > 0$, $\Sigma + \varepsilon I_{C'} \succ \mathbf{0}$. $\frac{d}{dt} \log \det \Sigma = \text{tr}(\Sigma^{-1} \dot{\Sigma})$, we obtain

$$\dot{h} = \frac{1}{2} \text{tr}(\Sigma^{-1} \dot{\Sigma}). \tag{S1}$$

By the same identity,

$$\dot{\mathcal{L}}_{\text{cov}} = -\frac{1}{C'} \text{tr}\left((\Sigma + \varepsilon I_{C'})^{-1} \dot{\Sigma}\right). \tag{S2}$$

Because $(\Sigma + \varepsilon I_{C'})^{-1} \preceq \Sigma^{-1}$ in the Löwner order (for $\varepsilon > 0$), we have

$$\text{tr}\left((\Sigma + \varepsilon I_{C'})^{-1} \dot{\Sigma}\right) \leq \text{tr}(\Sigma^{-1} \dot{\Sigma}). \tag{S3}$$

Combining (S1)–(S3) yields $\dot{h} \geq -\frac{C'}{2} \dot{\mathcal{L}}_{\text{cov}}$.

If the optimisation rule ensures $\dot{\mathcal{L}}_{\text{cov}} \leq 0$ (e.g. gradient descent or any monotone line search), then the inequality gives $\dot{h} \geq 0$. Equality holds only when $\dot{\mathcal{L}}_{\text{cov}} = 0$, which, under differentiability, implies the gradient of the loss is zero. Therefore entropy increases strictly whenever the loss decreases strictly. \square

I Detailed Experimental Setup for Empirical Analysis

This appendix provides additional details on the synthetic experiments described in Section 3.2, including data generation, model architectures, training procedure, and evaluation.

I.1 Synthetic Data Generation

We generate multivariate time series using a Vector Autoregression process:

$$z_{t+1} = Az_t + \varepsilon_{t+1}, \quad \varepsilon_{t+1} \stackrel{i.i.d.}{\sim} \mathcal{N}(\mathbf{0}, I),$$

where $z_t \in \mathbb{R}^C$, and the coefficient matrix $A \in \mathbb{R}^{C \times C}$ controls the temporal and inter-channel dependencies.

We consider the following dependency structures:

- **Independent:** A is a diagonal matrix with entries drawn independently from $[0.8, 1.0]$. Each channel evolves independently without influence from others.
- **Anti-Self:** A has zeros on the diagonal and off-diagonal entries drawn from $[0.5, 1.0]$. This ensures each channel is fully dependent on other channels but not on itself.

To ensure stability, we scale A so that its spectral radius is less than 1. Time series are simulated with $T = 100$ time steps and dimensionality $C \in \{100, 250, 2000\}$. The first 10 steps are discarded to reduce initialization bias.

I.2 Forecasting Task and Data Preparation

We define an autoregressive forecasting task where the model observes the past $L = 4$ time steps and predicts the next $H = 4$ steps:

$$\{z_{t-L+1}, \dots, z_t\} \mapsto \{z_{t+1}, \dots, z_{t+H}\}.$$

For each sequence, we construct overlapping sliding windows. The dataset is split into 80% training and 20% testing samples.

Before training, data is normalized using a channel-wise z-score computed over the training set:

$$\tilde{z}_t^{(i)} = \frac{z_t^{(i)} - \mu_i}{\sigma_i},$$

where μ_i and σ_i are the mean and standard deviation of channel i .

I.3 Model Architectures

We compare the following two models:

- **CI:** Each channel is modeled independently using a shared linear model. Input shape is $[B, L, C]$, and output shape is $[B, H, C]$. Each channel uses a shared linear layer: $\mathbb{R}^L \rightarrow \mathbb{R}^H$.
- **CD:** Each channel is first forecasted independently (as in CI), and the resulting output is then transformed using a shared linear layer across the channel dimension: $\mathbb{R}^{H \times C} \rightarrow \mathbb{R}^{H \times C}$.

Both models are implemented in PyTorch and trained using the Adam optimizer.

I.4 Training Details

Each model is trained for 100 epochs with a learning rate of 0.01 and batch size 32. We use mean squared error (MSE) as the loss function. To stabilize training, gradients are clipped with a maximum norm of 5. Models are trained on a single V100 GPU.

I.5 Evaluation Metrics

We report the mean squared error (MSE) averaged over all channels and forecast steps:

$$\text{MSE} = \frac{1}{HCN} \sum_{n=1}^N \sum_{h=1}^H \sum_{c=1}^C \left(\hat{z}_{t+h}^{(c)} - z_{t+h}^{(c)} \right)^2,$$

where N is the number of test samples.

J Computational Complexity

Notation C – number of channels (tokens in the *channel* dimension); T – look-back length (time steps); d – model width; h – number of heads; $r > 1$ – reduction ratio; $L = \lceil \log_r C \rceil$ – number of encoder/decoder stages. Before the first attention layer, both UCast and iTransformer apply a *single* linear map $\mathbf{W}_{\text{in}} \in \mathbb{R}^{T \times d}$ that compresses each length- T series to a d -dimensional embedding. Consequently, attention thereafter depends only on *channel counts*, not on T .

Hierarchical Latent Query Network. At stage ℓ the query length is $M_\ell = C/r^\ell$ and the key/value length is $C_{\ell-1} = C/r^{(\ell-1)}$. Scaled-dot-product attention therefore costs

$$\mathcal{T}_{\text{attn}}^{(\ell)} = \mathcal{O}(M_\ell C_{\ell-1} d/h) = \mathcal{O}\left(\frac{C^2 d}{h r^{2\ell-1}}\right).$$

Summing the geometric series over $\ell = 1, \dots, L$ gives the encoder cost

$$\mathcal{T}_{\text{enc}} = \mathcal{O}\left(\frac{C^2 d}{h r}\right).$$

Hierarchical Upsampling Network. The decoder is symmetric, so $\mathcal{T}_{\text{dec}} = \mathcal{O}(C^2 d/(h r))$. Hence the *overall* time complexity of UCast is

$$\boxed{\mathcal{T}_{\text{UCast}} = \mathcal{O}\left(\frac{C^2 d}{h r}\right)}.$$

Peak attention memory occurs in the first stage with $M_1 \times C = C^2/r$ score entries per head:

$$\boxed{\mathcal{M}_{\text{UCast}} = \mathcal{O}\left(\frac{C^2}{r}\right)}.$$

iTransformer iTransformer also compresses the time axis to width d and then applies full self-attention *once* over the C channel tokens:

$$\boxed{\mathcal{T}_{\text{iTrans}} = \mathcal{O}\left(\frac{C^2 d}{h}\right)}, \quad \boxed{\mathcal{M}_{\text{iTrans}} = \mathcal{O}(C^2)}.$$

Comparison The reduction ratio r governs the savings:

$$\frac{\mathcal{T}_{\text{UCast}}}{\mathcal{T}_{\text{iTrans}}} = \frac{1}{r}, \quad \frac{\mathcal{M}_{\text{UCast}}}{\mathcal{M}_{\text{iTrans}}} = \frac{1}{r}.$$

With a typical choice $r = 16$, UCast lowers both time and memory by a factor of 16 compared with a flat channel Transformer, yet still retains the expressive power of attention through its latent-query hierarchy.

K Dataset Description

Temp (Global Temp) and **Wind** (Global Wind). We adapt this dataset from Corrformer [50]. Global Temp&Wind dataset is from the National Centers for Environmental Information (NCEI) ⁴. This dataset contains the hourly averaged wind speed and hourly temperature of 3,850 stations (7,700 dimensions) around the world from 01/01/2019 to 12/31/2020, 17,544 timesteps in total. This dataset is well established. However, we find there are some constant columns in the datasets, which means the temp or wind speed never change. We remove these columns.

Solar (NREL Solar Power). NREL Solar Power is collected from National Renewable Energy Laboratory (NREL) ⁵. One of the most popular datasets for time series forecasting is Solar-Energy [20], which is sourced from NREL. However, it includes data from only 137 solar photovoltaic (PV) plants in Alabama, limiting the dataset to 137 dimensions. To increase the dimensionality, we collect data

⁴<https://www.ncei.noaa.gov/>

⁵<https://www.nrel.gov/grid/solar-power-data.html>

from 5,166 PV plants across 47 U.S. states, excluding Alaska, Hawaii, and North Dakota, using data from NREL. The data source is clean so we don't conduct further preprocessing on it.

Meters (Smart meters in London). We process half-hourly smart meter energy consumption data by loading data from multiple blocks, where each block represents a subset of meters, and aggregating energy consumption data for each meter. The energy unit is kWh/hh. The data is sorted chronologically and merged into a single dataset, consisting of *5,567 meters and 40,405 timesteps*. **First**, to address missing values introduced by the staggered installation of meters, we filter out records before 07/14/2012, as meters were installed at different times starting from 11/23/2011. We also ensure that only records with exact half-hour intervals are retained, resulting in a dataset of *5,567 meters and 28,512 timesteps*. **Second**, we remove meters that became operational after 07/14/2012 or stopped reporting before 02/28/2014, reducing the dataset to *4,213 meters while maintaining 28,512 timesteps*. **Third**, we count missing values and remove meters with more than 10 missing values. The remaining missing values are replaced with zero, yielding a final dataset of *2,899 meters and 28,512 timesteps*. The cleaned and processed dataset is then saved for further analysis.

Traffic-CA (LargeST-CA), **Traffic-GLA** (LargeST-GLA), **Traffic-GBA** (LargeST-GBA). The source of this dataset is the Caltrans Performance Measurement System (PeMS)⁶, and we utilize its preprocessed version[24]. **LargeST-CA** encompassing a total of 8,600 sensors in California and each sensor contains five years of traffic flow data (from 2017 to 2021) with a 5-minute interval, resulting in a total of 525,888 time frames. **LargeST-CA consists of three subsets: (1) LargeST-GLA** includes 3,834 sensors installed across five counties in the Greater Los Angeles (GLA) area: Los Angeles, Orange, Riverside, San Bernardino, and Ventura. **(2) LargeST-GBA** contains 2,352 sensors distributed across 11 counties in the Greater Bay Area (GBA): Alameda, Contra Costa, Marin, Napa, San Benito, San Francisco, San Mateo, Santa Clara, Santa Cruz, Solano, and Sonoma. **(3) LargeST-SD**, the smallest subset, consists of 716 sensors located exclusively in San Diego County. Since LargeST-SD has only 716 dimensions, we do not include it in our benchmark. For the 525,888 original time frames, we aggregate the data into 1-hour intervals, resulting in 43,824 time frames. We then remove sensors with more than 100 missing (NaN) values, and apply linear interpolation to fill the remaining missing values.

Neurolib. Simulations made use of the Neurolib code [4]. We utilize the brain structure in ABIDE dataset [9].

SIRS. Simulations extend the classical SIR model [3] by incorporating temporary immunity, resulting in dynamic transitions among Susceptible, Infected, and Recovered groups within a single region. To enhance realism, parameter noise, and seasonal variation are included. For multiple regions, each compartment has a fixed transfer rate between regions to simulate commuting and spatial transmission dynamics.

Air Quality (Chinese Air Quality). This dataset includes 7 air quality indicators: *AQI, CO, NO₂, O₃, PM₁₀, PM_{2.5}, and SO₂* of 786 distinct cities in China. We remove dimensions with more than 100 missing values and interpolate other dimensions linearly, resulting in 1,106 dimensions.

SP500 (S&P 500 Index). The S&P 500 is a stock market index maintained by S&P Dow Jones Indices⁷. It consists of 503 common stocks issued by 500 large-cap companies traded on American stock exchanges. We use *yfinance*⁸, a Python package for financial data retrieval, to download market data for these stocks from Yahoo Finance⁹. We select the latest S&P 500 company list (as of 03/14/2025) and extract daily market data spanning the past 30 years (7,553 days). To ensure data consistency, we retain only the companies that were publicly traded 30 years ago, reducing the dataset to 295 companies. For each company, we extract five key market variables: Open, Close, High, Low, and Volume, resulting in a total of 1,475 dimensions.

M5. We adapt this dataset from a Kaggle competition [18]. It covers stores in three U.S. states, i.e. California, Texas, and Wisconsin, and includes item-level sales data, department and product category details, and store information. The dataset records daily sales for each item from 07/01/2015 to 06/30/2022 (a total of 1,947 days) across different departments and stores, resulting in 30,490 time

⁶<https://pems.dot.ca.gov/>

⁷<https://www.spglobal.com/spdji/en/>

⁸<https://github.com/ranaroussi/yfinance>

⁹<https://finance.yahoo.com/>

series. Due to its sparsity (i.e., a large number of zero values), we aggregate sales by summing each item’s sales across all departments and stores, reducing the dataset to 3,049 aggregated items.

Atec. The dataset consists of 1589 traffic data collected every 10 minutes for different zones of different applications. We remove the dimensions that include more than 10 missing values and conduct interpolation for the remaining dimensions.

Measles (Measles England). The measles dataset [31, 28, 27], contains biweekly measles infections from 387 regions across England and Wales from 1944–1965. For each region, the dataset includes three features: inferred infections, population, and suspected cases, resulting in 1,161 dimensions.

Wiki-20k (Wikipedia Web Traffic) The dataset is adapted from the Monash Time Series Forecasting Repository ¹⁰. It comprises 145,063 time series representing web traffic for various Wikipedia pages from July 1, 2015, to June 30, 2022 (2,557 days). This dataset is an extended version of the one used in the Kaggle Wikipedia Web Traffic Forecasting Competition ¹¹. Due to data sparsity, we remove the Wikipedia pages containing NaN values, resulting in a final dataset of 112,333 Wikipedia pages, each corresponding to one dimension. Due to the original dataset’s dimension is too large and is not correlated, we select the first 20k dimensions to construct Wiki-20k dataset for evaluation.

Mobility (Google Community Mobility). The Community Mobility dataset [15] aims to assist in analyzing the impact of COVID-19 on community movement patterns. The dataset covers movement trends over time (from February 15, 2020, to October 15, 2022, spanning 974 days) across 4,334 regions in different countries. It categorizes mobility data into **six** place types: **retail and recreation** (restaurants, cafes, shopping centers, theme parks, museums, libraries, and movie theaters), **groceries and pharmacies** (grocery stores, food warehouses, farmers markets, specialty food shops, drug stores, and pharmacies), **parks** (local and national parks, public beaches, marinas, dog parks, plazas, and public gardens), **transit stations** (subway, bus, and train stations), **workplaces** (places of employment), and **residential** (places of residence). The dataset initially consists of 26,004 dimensions, derived from the six place categories across 4,334 regions. However, due to data sparsity, we exclude regions containing NaN values, reducing the dataset to 971 regions and 5,826 dimensions. The values in the dataset represent changes in visit frequency and duration of stay at various locations relative to the baseline (i.e. the median value for the same day of the week during the five-week period from January 3 to February 6, 2020.). These changes are computed using aggregated and anonymized data, similar to the methodology employed in Google Maps to estimate popular visit times.

L Channel Correlation Statistic

We follow TFB [38] to compute channel correlation. In multivariate time series, different variables often share common temporal patterns due to underlying shared factors. To quantify this, we extract 22 features per channel using Catch22 [29]. These features serve as fixed-length representations of each time series channel. We then compute the pairwise Pearson correlation coefficients [8] between all channel representations and report the mean and variance. The results are shown in the “*Correlation*” column of Table 2. All datasets exhibit high average channel correlation, confirming the presence of strong inter-variable dependencies in these high-dimensional time series.

M Implementation Details

Metric Details. We use Mean Square Error (MSE) and Mean Absolute Error (MAE) as our evaluation metrics, following [25, 30, 44, 48, 49, 58, 53]:

$$\text{MSE} = \frac{1}{S \times C} \sum_{i=1}^S \sum_{j=1}^C (\mathbf{Y}_{ij} - \hat{\mathbf{Y}}_{ij})^2, \quad (8)$$

$$\text{MAE} = \frac{1}{S \times C} \sum_{i=1}^S \sum_{j=1}^C |\mathbf{Y}_{ij} - \hat{\mathbf{Y}}_{ij}|. \quad (9)$$

¹⁰<https://zenodo.org/records/7370977>

¹¹<https://www.kaggle.com/c/web-traffic-time-series-forecasting/data>

Here, $\mathbf{Y} \in \mathbb{R}^{S \times C}$ represents the ground truth, and $\hat{\mathbf{Y}} \in \mathbb{R}^{S \times C}$ represents the predictions. S denotes the future prediction length, C is the number of channels, and Y_{ij} indicates the value at the i -th future time point for the j -th channel.

Experiment Details. All experiments are implemented in PyTorch [37] and conducted on a cluster equipped with 8 NVIDIA A100 GPUs. The baselines are trained using their default configurations as reported in their respective papers, and with further hyperparameter searching (Learning Rate in $\{0.01, 0.001, 0.0001\}$, Input Sequence Length T in $\{3 \times S, 4 \times S, 5 \times S\}$), where S is prediction length. ADAM optimizer [19] is used with MSE loss for the training of all the models. We apply early stopping with a patience value of 5 epochs. The batch size is initially set to 32. If an out-of-memory (OOM) error occurs, the batch size is automatically halved until the issue is resolved. For U-CAST, we default to using non-stationary [26] normalization for all datasets. We default to set the batch size to 128, the number of layers L to 2, the hidden dimension d to 512, and the reduction ratio r to 16 for all the datasets. Additional detailed U-CAST model configuration information is presented in Table 6. We conduct hyperparameter sensitivity analysis in Appendix N.

Table 6: U-CAST hyperparameters used for each dataset.

Dataset	Learning Rate	Input Sequence Length T	α
Atec	0.002	$3 \times S$	0.001
Air Quality	0.0005	$4 \times S$	1
Temp	0.0005	$3 \times S$	0.01
Wind	0.001	$4 \times S$	0.001
Mobility	0.002	$4 \times S$	10
Traffic-CA	0.001	$4 \times S$	1
Traffic-GBA	0.001	$4 \times S$	0.01
Traffic-GLA	0.001	$4 \times S$	1
M5	0.0005	$4 \times S$	0.1
Measles	0.0005	$3 \times S$	0.001
Neurolib	0.002	$4 \times S$	0.001
Solar	0.0005	$4 \times S$	0.001
SIRS	0.0005	$4 \times S$	1
Meters	0.0005	$4 \times S$	0.001
SP500	0.001	$3 \times S$	1
Wiki-20k	0.0005	$4 \times S$	10

N Hyperparameter Sensitivity Analysis

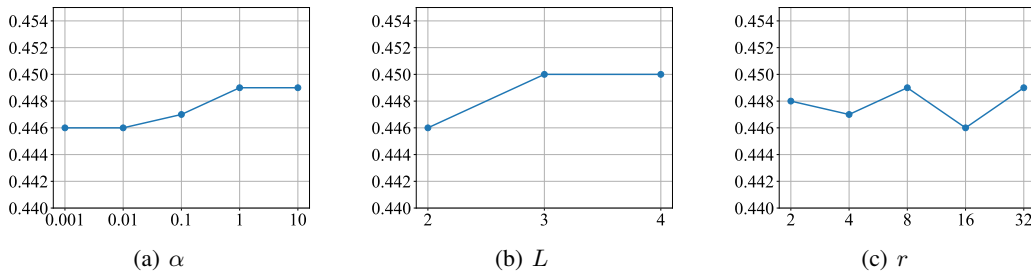


Figure 5: Performance (MSE) on China Air Quality dataset under different hyperparameters.

Sensitivity Analysis of the full-rank regularization strength α . We analyze how the regularization coefficient α affects the performance of U-CAST by varying it across several orders of magnitude. As shown in Figure 5 (a), the model achieves the best performance when α is set to a small value (0.001–0.01). As α increases, the forecasting error (MSE) gradually rises, suggesting that overly strong regularization may overconstrain the channel representations, thereby reducing the model’s ability to capture informative structures. Based on this analysis, we select $\alpha = 0.01$ for a good balance between disentanglement and flexibility.

Sensitivity Analysis of the number of hierarchical layers L . We evaluate the effect of the number of hierarchical latent query layers L on forecasting performance, where a lower mean squared error (MSE) indicates better accuracy. As shown in Figure 5 (b), increasing L from 2 to 3 reduces the MSE, indicating worse performance. This suggests that deeper hierarchies may not capture more useful structure and could lead to redundancy or overfitting. Based on this analysis, we set $L = 2$ in our main experiments.

Sensitivity Analysis of the reduction ratio r . We investigate how the reduction ratio r , which determines the compression of channel representations at each layer, influences performance. As shown in Figure 5 (c), the model achieves relatively stable performance across a wide range of r values. However, extremely large or small values can lead to slight degradation. For instance, very low reduction (e.g., $r = 2$) leads to higher computational cost without performance gain, while aggressive reduction (e.g., $r = 32$) may discard useful information. We find that $r = 16$ offers a favorable trade-off between efficiency and accuracy.

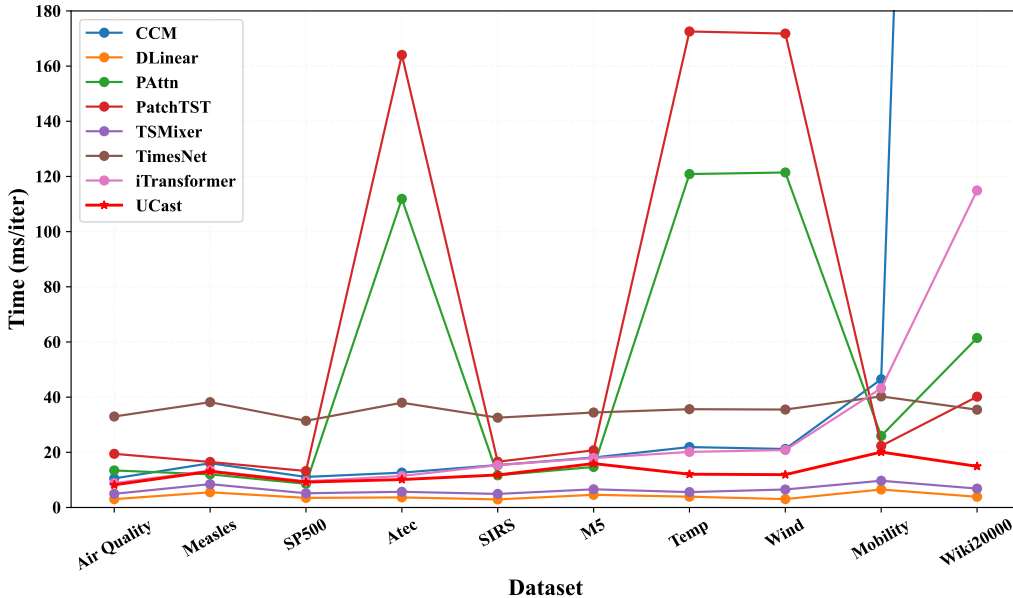


Figure 6: Training time across datasets.

O Efficiency

We compare the training time per batch with recent state-of-the-art models in Figure 6. The x-axis represents different datasets, arranged from left to right in order of increasing dimensionality. The results show that: (1) U-CAST consistently achieves favorable training efficiency across varying dimensionalities; (2) As dimensionality increases, the efficiency advantage of U-CAST over other non-linear methods becomes more pronounced; (3) The efficiency of CI-based methods such as PAttn and PatchTST is affected by both the channel and temporal dimensions. When the channel dimensionality becomes very large, as in the Wiki20000 dataset, its efficiency degrades significantly; (4) The efficiency of CD-based methods, including iTransformer, CCM, and U-CAST, is primarily influenced by the number of input channel dimensions.

P Ablation Study

As U-CAST integrates two core components, the Hierarchical Latent Query Network and the Hierarchical Upsampling Network, we assess their individual contributions through ablation studies. Specifically, we evaluate the impact of: (1) **w/o hierarchical** by retaining only a single layer for dimensionality reduction, (2) **w/o latent query** by setting \mathbf{Q}_ℓ requires_grad=False, and (3) **w/o up-**

Table 7: Ablation study on different components of U-CAST. Each model is evaluated on 16 datasets using MSE and MAE. The best performance is highlighted in **red**, and the second-best is underlined.

Dataset	U-CAST		w/o \mathcal{L}_{cov}		w/o Hierarchical		w/o Latent Query		w/o Upsampling	
	MSE	MAE	MSE	MAE	MSE	MAE	MSE	MAE	MSE	MAE
Atec	0.287	0.280	<u>0.311</u>	<u>0.297</u>	0.319	0.306	0.308	0.296	0.306	0.292
Air Quality	0.446	0.430	<u>0.461</u>	<u>0.444</u>	0.447	0.431	0.451	0.434	0.451	0.434
Temp	0.262	0.383	<u>0.273</u>	<u>0.395</u>	0.272	0.392	0.280	0.398	0.294	0.410
Wind	1.104	0.692	1.115	0.701	<u>1.110</u>	<u>0.695</u>	1.106	0.692	1.109	<u>0.693</u>
Mobility	0.315	0.317	0.336	0.332	<u>0.316</u>	<u>0.319</u>	0.326	0.323	0.327	0.324
Traffic-CA	0.061	0.131	0.072	0.144	<u>0.062</u>	0.138	<u>0.062</u>	0.136	<u>0.062</u>	<u>0.133</u>
Traffic-GBA	0.059	0.126	0.070	0.137	<u>0.060</u>	0.130	<u>0.060</u>	0.130	<u>0.060</u>	<u>0.127</u>
Traffic-GLA	0.060	0.132	0.071	0.144	<u>0.061</u>	0.136	<u>0.061</u>	0.135	<u>0.061</u>	<u>0.134</u>
M5	3.501	0.849	<u>3.520</u>	0.861	3.566	<u>0.854</u>	3.516	0.852	3.597	0.860
Measles	0.010	0.042	0.022	0.061	0.019	0.054	<u>0.011</u>	<u>0.051</u>	0.014	0.063
Neurolib	1.750	0.350	<u>1.770</u>	0.362	1.818	0.370	1.813	<u>0.358</u>	<u>1.756</u>	0.355
Solar	<u>0.172</u>	0.246	0.182	<u>0.242</u>	0.173	0.239	0.175	0.237	0.167	0.222
SIRS	0.007	0.052	0.038	0.119	0.008	<u>0.056</u>	<u>0.008</u>	0.057	0.035	0.126
Meters	0.943	<u>0.551</u>	0.957	0.563	0.950	0.558	<u>0.945</u>	0.552	0.946	0.550
SP500	0.555	0.328	<u>0.561</u>	0.338	0.562	<u>0.333</u>	0.566	0.335	0.597	0.349
Wiki20000	10.273	0.302	<u>10.520</u>	0.321	10.459	0.309	10.509	<u>0.310</u>	10.527	<u>0.310</u>

sampling by using a simple linear projection to restore channel dimension. In addition, we examine the role of the covariance full-rank regularisation by **w/o** \mathcal{L}_{cov} , i.e., setting $\alpha = 0$.

Table 7 shows that removing any component generally degrades U-CAST’s performance, confirming their necessity. **First**, *w/o latent query* still performs well on some datasets (e.g., NREL Solar Power), likely due to high inter-variable correlation (0.998), where random projections suffice. **Second**, *w/o upsampling* unexpectedly improves performance on NREL, suggesting that encoder representations are already sufficient and further decoding may introduce redundancy or overfitting. **Third**, removing the covariance regularization has the largest impact on structured datasets like SIRS (MSE rises from 0.007 to 0.038), showing its importance in enforcing feature decorrelation.